Journal of Sedimentary Research

Journal of Sedimentary Research, 2020, v. 90, 1175–1197
Research Article
DOI: http://dx.doi.org/10.2110/jsr.2020.52

EARLY SEVIER OROGENIC DEFORMATION EXERTED PRINCIPAL CONTROL ON CHANGES IN DEPOSITIONAL ENVIRONMENT RECORDED BY THE CRETACEOUS NEWARK CANYON FORMATION

ANNE C. FETROW,[1] KATHRYN E. SNELL,[1] RUSSELL V. DI FIORI,[2] SEAN P. LONG[2] AND JOSHUA W. BONDE[3]
[1]*University of Colorado–Boulder, 2200 Colorado Avenue, Boulder, Colorado 80309, U.S.A.*
[2]*Idaho Geological Survey, Morrill Hall, University of Idaho, Moscow, Idaho 83844, U.S.A.*
[3]*Nevada Science Center, 331 South Water Street, Unit D, Henderson, Nevada 89015, U.S.A.*
e-mail: anne.fetrow@colorado.edu

ABSTRACT: **Terrestrial sedimentary archives record critical information about environment and climate of the past, as well as provide insights into the style, timing, and magnitude of structural deformation in a region. The Cretaceous Newark Canyon Formation, located in central Nevada, USA, was deposited in the hinterland of the Sevier fold–thrust belt during the North American Cordilleran orogeny. While previous research has focused on the coarser-grained, fluvial components of the Newark Canyon Formation, the carbonate and finer-grained facies of this formation remain comparatively understudied. A more complete understanding of the Newark Canyon Formation provides insights into Cretaceous syndeformational deposition in the Central Nevada thrust belt, serves as a useful case study for deconvolving the influence of tectonic and climatic forces on sedimentation in both the North American Cordillera and other contractional orogens, and will provide a critical foundation upon which to build future paleoclimate and paleoaltimetry studies.**

We combine facies descriptions, stratigraphic measurements, and optical and cathodoluminescence petrography to develop a comprehensive depositional model for the Newark Canyon Formation. We identify six distinct facies that show that the Newark Canyon Formation evolved through four stages of deposition: 1) an anastomosing river system with palustrine interchannel areas, 2) a braided river system, 3) a balance-filled, carbonate-bearing lacustrine system, and 4) a second braided river system. Although climate undoubtedly played a role, we suggest that the deposition and coeval deformation of the synorogenic Newark Canyon Formation was in direct response to the construction of east-vergent contractional structures proximal to the type section. Comparison to other contemporary terrestrial sedimentary basins deposited in a variety of tectonic settings provides helpful insights into the influences of regional tectonics, regional and global climate, catchment characteristics, underlying lithologies, and subcrop geology in the preserved sedimentary record.

INTRODUCTION

Terrestrial sedimentary archives provide important insights into the tectonic setting in which they were deposited including the style and timing of deformation, and the climate conditions of the basin at the time of deposition (Burbank et al. 1988; Fillmore and Middleton 1989; Quigley et al. 2007). Piggyback basins, defined as a sedimentary basins that form on the hanging wall of an active thrust fault, are particularly useful for constraining the type, inception, and longevity of deformation along orogenic fronts (Ori and Friend 1984; Lawton and Trexler 1991; Coogan 1992; Lawton et al. 1993; DeCelles and Coogan 2006). Piggyback basins characteristically record a mosaic of discontinuous facies as sedimentation patterns respond to developing intrabasinal deformation structures (Ori and Friend 1984; Lawton and Trexler 1991). Research into terrestrial piggyback systems that include major carbonate-bearing components has recently been reinvigorated because of their potential to preserve evidence of regional and continental-scale tectonic deformation (e.g., Quigley et al. 2007; Druschke et al. 2011; Long et al. 2014; Sacristán-Horcajada et al. 2016; Di Fiori et al. 2020). Additionally, they can yield information about environmental, vegetative, and climatic conditions of past landscapes (Carroll and Bohacs 1999; Bohacs et al. 2000; Freytet and Verrechia 2002; Alonso-Zarza 2003; Leng and Marshall 2004; Gierlowski-Kordesch 2009), and possible hydrocarbon accumulations (e.g., Abrahão and Warme 1990; Herlinger et al. 2017). Analyses of syncontractional sediments commonly focus on the coarse-grained facies in sedimentological records because these lithologies are directly linked to changes in energy levels, and therefore provide insight into the relationship between sedimentation and deformation. Additionally, often coarse-grained lithologies are preferentially preserved and exposed. However, the need for a more nuanced perspective on the interaction of climate and tectonics has become apparent as our understanding of these dynamics throughout the geologic past has improved. Paying the same attention to the carbonate and finer-grained facies of these records can provide critical detail about physical depositional processes, as well as chemical conditions of a system that can be used to unravel some of the more enigmatic tectonic and climate questions.

From the Jurassic to the Paleogene, subduction of the Farallon Plate under the western margin of the North American continent caused contractional deformation that built a vast mountain belt (Jordan and

Published Online: September 2020
 1527-1404/20/090-1175

Allmendinger 1986; Burchfiel et al. 1992; DeCelles 2004; Dickinson 2004; DeCelles and Coogan 2006; Yonkee and Weil 2015). While there has been extensive study of the North American Cordillera, many questions remain about the style and magnitude of deformation in the system in different places during a range of times (e.g., Taylor et al. 2000; DeCelles and Coogan 2006; DeCelles 2009; Long 2015; Long et al. 2014, 2015). For example, the timing of uplift, magnitude of surface elevation, and possible decoupling of crustal thickening with surface uplift are still debated for the Sevier hinterland, which is often referred to as the "Nevadaplano" after comparisons with the modern Altiplano–Puna plateau located in the modern Andean cordillera (Coney and Harms 1984; Chase et al. 1998; Dilek and Moores 1999; DeCelles 2004; DeCelles and Coogan 2006; Ernst 2009; Snell et al. 2014; Long et al. 2015).

The Early to mid-Cretaceous Newark Canyon Formation (Knc) records sedimentation in the hinterland of the Sevier fold–thrust belt during the early stages of Sevier orogenesis and is a well-situated archive with which we can better answer questions about the style of deformation and the climate in the region (Vandervoort 1987; Vandervoort and Schmitt 1990; Druschke et al. 2011; Long et al. 2014). The Newark Canyon Formation was deposited in fluvial, fluvio-lacustrine, and lacustrine environments that drained the Sevier hinterland towards the foreland to the east (Vandervoort 1987). Previous work has focused principally on the coarse-grained siliciclastic deposits, and although this work developed an important sedimentary framework for the Newark Canyon Formation, it lacks thorough description of the carbonate and finer-grained siliciclastic facies that dominate many phases of deposition in the basin. These carbonate and fine-grained facies not only can contribute to our understanding of the depositional history of the Newark Canyon Formation but also can help constrain the development of the Sevier orogenic system and North American Cordillera and provide insights into the evolution of other compressional tectonic settings, such as the Andean orogenic system. Additionally, understanding the driving forces of sedimentation in the Sevier hinterland will contribute to interpreting paleoenvironmental and paleoclimatic change in the U.S. cordillera during the Cretaceous.

In this study, we focus on the palustrine and lacustrine carbonate lithofacies from the type section (TS) of the Newark Canyon Formation in order to more fully assess the depositional conditions under which these units formed. Adding to the work of Vandervoort (1987), we develop a revised depositional model that broadens our understanding of the environmental conditions of mid-latitude North America during the Albian to Cenomanian in the Cretaceous, as well as contextualizes future studies on the paleoclimate based on the geochemistry of these sedimentary archives and other similar formations. In combination with recent structural studies, this revised depositional history suggests that most of the environmental change in the type section was driven by the tectonic development of the basin during early stages of North American Cordilleran orogenesis.

BACKGROUND

Geologic Setting

Spatially isolated exposures of the Newark Canyon Formation are spread across a narrow N–S band ~ 150 km long throughout central Nevada (Fig. 1) (Nolan et al. 1956, 1974; Nolan and Hunt 1962; Long et al. 2014). The Newark Canyon Formation was deposited in the hinterland of the Cordilleran orogen, which was constructed during the Jurassic to Paleogene as a result of subduction of the Farallon Plate under the North American continent (Dewey and Bird 1970; Jordan and Allmendinger 1986; DeCelles 2004; Dickinson 2004; Yonkee and Weil 2015). This hinterland region is bounded by the Sierra Nevada magmatic arc to the west and the Sevier fold–thrust belt to the east (Fig. 1) (DeCelles 2004; DeCelles and Coogan 2006; Wells et al. 2012; Long et al. 2014).

The Central Nevada thrust belt (CNTB) is a structural province in the retroarc region and is defined by a north-trending series of east-vergent thrust faults and folds that branches northward off of the Sevier fold–thrust belt (SFTB) in southern Nevada (Taylor et al. 2000; Long et al. 2012, 2014, 2015). At the latitude of the town of Eureka (~ 39° N), CNTB deformation built the Eureka Culmination, a north–south-trending anticline that is interpreted as a fault-bend fold constructed above a blind thrust that can be traced for approximately 100 km through central Nevada and is estimated to have had an wavelength of ~ 20 km and an amplitude of ~ 4.5 km (Long et al. 2014; Long 2015, 2019). Exposures of the Newark Canyon Formation in the Diamond Mountains, which includes the type section, are interpreted to have been deposited in piggyback basins that formed on the eastern flank of the Eureka Culmination (Fig. 1) (Vandervoort 1987; Druschke et al. 2011; Long et al. 2014). This being the case, deformation along the Eureka Culmination would have played an important role in determining the timing and style of deformation in these basins.

Climatic Setting

Climate also plays a critical role in sedimentation by influencing physical and chemical weathering mechanisms and rates through the timing and style of precipitation and mean annual and range of temperatures. The climate during the Cretaceous period is characterized as a greenhouse climate with high atmospheric CO_2 concentrations and elevated global mean temperatures (Barron and Washington 1982; Royer 2006; Takashima et al. 2006; Pagani et al. 2013; Wang et al. 2014; Huber et al. 2018). During the time of deposition of the Newark Canyon Formation, TEX_{86} estimates of sea-surface temperatures suggest a lower equator-to-pole temperature gradient than today (Littler et al. 2011). A compilation of foraminiferal $\delta^{18}O$ values deposited at middle to upper bathyal paleodepths in southern high latitudes show that there were warm conditions throughout the Albian (~ 113 to 100 Ma) followed by extreme warmth during the mid-Turonian (~ 91 Ma) (Huber et al. 2018). Atmospheric CO_2 concentrations are estimated to have ranged between 600 and 1000 ppmv for the Aptian to Albian based on $\delta^{13}C$ from a succession of carbonate-bearing paleosols from central Utah, USA (Ludvigson et al. 2015).

In addition to increased global temperatures and atmospheric CO_2 concentrations, Cretaceous climate is hypothesized to have had an invigorated hydrologic cycle, meaning that areas of high precipitation would have become wetter and arid areas would have become drier (Barron and Washington 1982; Ufnar et al. 2004; Held and Soden 2002, 2006; Pagani et al. 2013). It is hypothesized that individual precipitation events would have been more "extreme," meaning that more precipitation would fall per event. This invigoration of the hydrologic cycle would have been particularly notable in mid-latitude continental interiors and would likely have led to significant changes in erosion rates and the timing and frequency of erosional events (Barron et al. 1989; Suarez et al. 2011; Burgener et al. 2019).

Previous Sedimentological Work

The Newark Canyon Formation is poorly exposed and commonly obscured by a deep overlying red soil with dense vegetative cover (Nolan and Hunt 1962; Vandervoort 1987). The Newark Canyon Formation was previously described throughout five exposures in the Diamond Mountains and Fish Creek Range in east-central Nevada and this work focused mainly on the coarse-grained siliciclastic facies (Vandervoort 1987). Informal members were assigned to the type section in the southern Diamond Mountains by Vandervoort (1987) which include the "basal conglomerate/mudstone, lower fine-grained assemblage, middle sandstone, upper conglomerate, and upper carbonaceous assemblage." More recent work

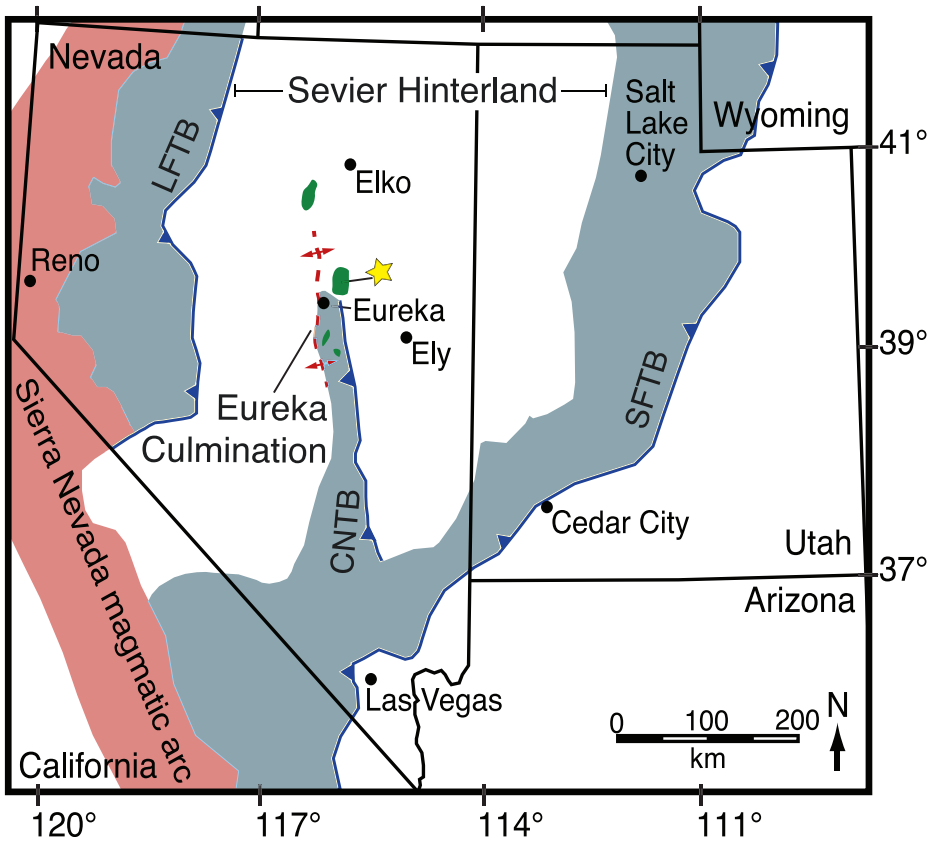

FIG. 1.—Regional map adapted from Long et al. (2014) showing approximate Mesozoic deformation fronts (blue lines) of Nevada, Utah, Wyoming, and eastern California. Spatial extents of the deformation fronts of major thrust systems are shaded. Location of the Sierra Nevada magmatic arc is from Van Buer et al. (2009). Abbreviations: SFTB, Sevier fold–thrust belt; CNTB, Central Nevada thrust belt; and LFTB, Luning–Fencemaker thrust belt. The yellow star indicates the location of the type section of the Newark Canyon Formation. Green shading indicates exposures of the Newark Canyon Formation throughout Nevada based on (Vandervoort and Schmitt 1990; Long et al. 2014; Di Fiori et al. 2020). The red line delineates the approximate location of the Eureka Culmination along the Central Nevada thrust belt near the town of Eureka.

by Di Fiori and others (2020) assigns five mappable members to the Newark Canyon Formation in the South Diamond Mountains (Knc1–Knc5) (Fig. 2). These mappable units stack conformably throughout the type section, except for two notable exceptions. There are progressive unconformities within Knc3 conglomerate beds where shallower-dipping beds (~ 17° W) overlie steeper-dipping beds (~ 40° W) that are interpreted as growth strata. Also, there is an angular unconformity at the base of Knc5 where Knc5 is ~ 10–20° shallower than units below. This likely indicates a preservation hiatus up to ~ 10 My (Fig. 3A) (Di Fiori et al. 2020).

Throughout this study for clarity, we integrate our described facies and depositional stages to these five mappable members. These lithologic divisions generally indicate that the Newark Canyon Formation was deposited in fluvial and lacustrine settings characterized by highly variable flow regimes. Cobble orientation and crossbedding indicate an east-flowing fluvial system, which suggests a sediment source to the west (Vandervoort and Schmitt 1990; Vandervoort 1987). The likely source for the sediment was the Eureka Culmination, which was located a few tens of kilometers to the west of the type section (Long et al. 2014).

Constraints on Depositional Age

The type section unconformably overlies the Permian Carbon Ridge Formation and is unconformably overlain by Tertiary volcanics and megabreccias (Nolan et al. 1956; Nolan and Hunt 1962; Strawson 1981; Vandervoort 1987; Druschke et al. 2011). Early Cretaceous freshwater faunas, such as unionids, gastropods, ostracods, fish fossils, and floras, such as charophytes and other plant macrofossils, are well documented in early studies of the Newark Canyon Formation (MacNeil 1939; David 1941; Nolan et al. 1956; Fouch 1979). Based on these fossils, the depositional age of the Newark Canyon Formation type section exposure was estimated to be Aptian–Albian (ca. 126 to 100 Ma) (Nolan et al. 1956; Smith and Kettner 1976; Fouch et al. 1979). More recent paleontology in the Newark Canyon Formation throughout Nevada has expanded the faunal list to include a gar fish (Lepisosteidae), a turtle genus *Glyptops*, a member of the freshwater shark family Hybodontidae, two types of crocodilians, and a number of dinosaur families, and is interpreted as Early Cretaceous based on this faunal assemblage (Bonde et al. 2015).

From the type section, initial U-Pb dating of zircons from a sandstone from the middle part of the section yielded a maximum depositional age (MDA) of ~ 121 Ma, and a depositional age of 116.1 ± 1.6 Ma from a reworked water-laid tuff near the top of the section (Druschke et al. 2011). More recent U-Pb zircon geochronology has refined those ages; new dates from the same water-laid tuff yielded a concordia age of a coherent population of zircons at 103.0 ± 0.7 Ma (Di Fiori et al. 2020). Additionally, Di Fiori et al. (2020) yielded refined MDA estimates for the type section based on U-Pb zircon geochronology of detrital zircons. The results provide a MDA of 113.7 ± 2.3 Ma for Knc1, a MDA of 112.92 ± 1.0 Ma for Knc3, and a MDA of 98.6 ± 1.9 Ma for Knc5 (Fig. 3A) (Di Fiori et al. 2020). Note that the MDA used for Knc1 was generated from a basal mudstone sample located ~ 10 km north of the type section, in the west Hildebrand exposure of the Newark Canyon Formation.

MATERIALS AND METHODS

We measured and described stratigraphic sections using a Jacob's staff and collected hand samples along four transects (labeled TS2-TS5) in the type section of the Newark Canyon Formation (Fig. 2). Hand samples, GPS coordinates, and sample and exposure photos of carbonate and mudstone facies were taken approximately every 0.5 m where exposure allowed (Table 1). Representative hand samples of sandstone and conglomerate facies were sampled selectively throughout the section. Outcrop colors were assigned color codes using the Rock Color Chart (Goddard et al.

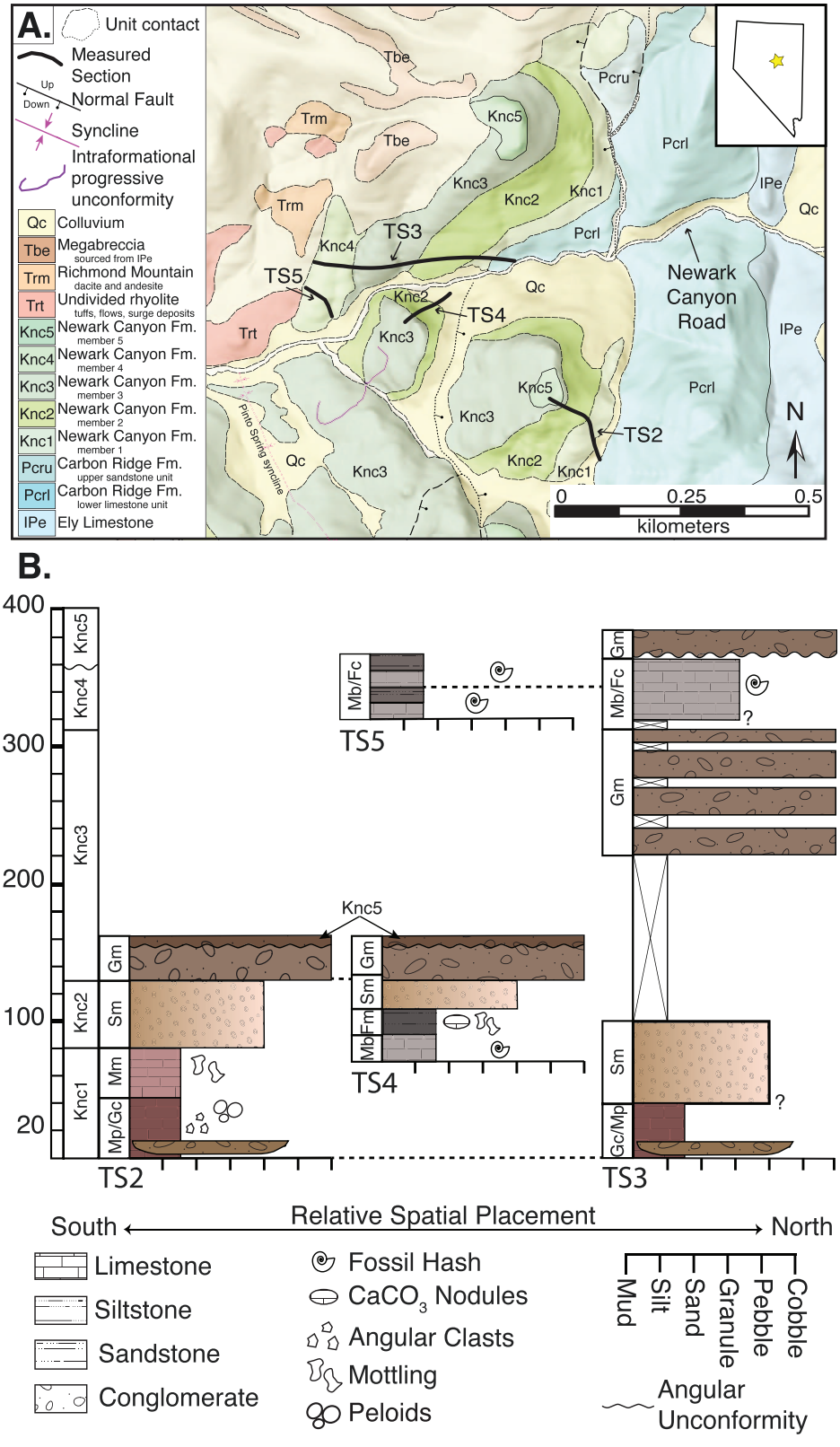

FIG. 2.—**A)** Structural map of the type section located along Newark Canyon Road showing the five measured sections, indicated with thick black lines (TS2–TS5). In the upper right corner, the yellow star in the Nevada outline map indicates approximate location of the type section. Base map modified from Di Fiori et al. (2020). Abbreviations: Newark Canyon Formation mappable member name, in stratigraphic order: Knc1, lower micrite and interbedded conglomerate; Knc2, lower sandstone; Knc3, middle conglomerate; Knc4, upper micrite; and Knc5, upper conglomerate. For symbols representing unit contacts, normal faults, and syncline maps, the large dashes show approximate location and small dashes indicate that location is concealed but inferred. **B)** Generalized stratigraphic columns (m) for sections TS2–TS5 placed in relative geographic position to illustrate how sections are spatially associated. Facies abbreviations relate to facies descriptions in the Results section.

1984). We describe mottling using the classification defined by the United States Department of Agriculture Natural Resources Conservation Services, where "distinct" contrast refers to color that is readily seen but contrasts only moderately with the color with which it is compared (NRCS Soils Staff 2017). Our results build on the work done by Vandervoort (1987) and use the Miall (1977b) classification system for siliciclastic facies to best compare to previous descriptions. Carbonate facies descriptions follow the practical classification of limestones from Folk

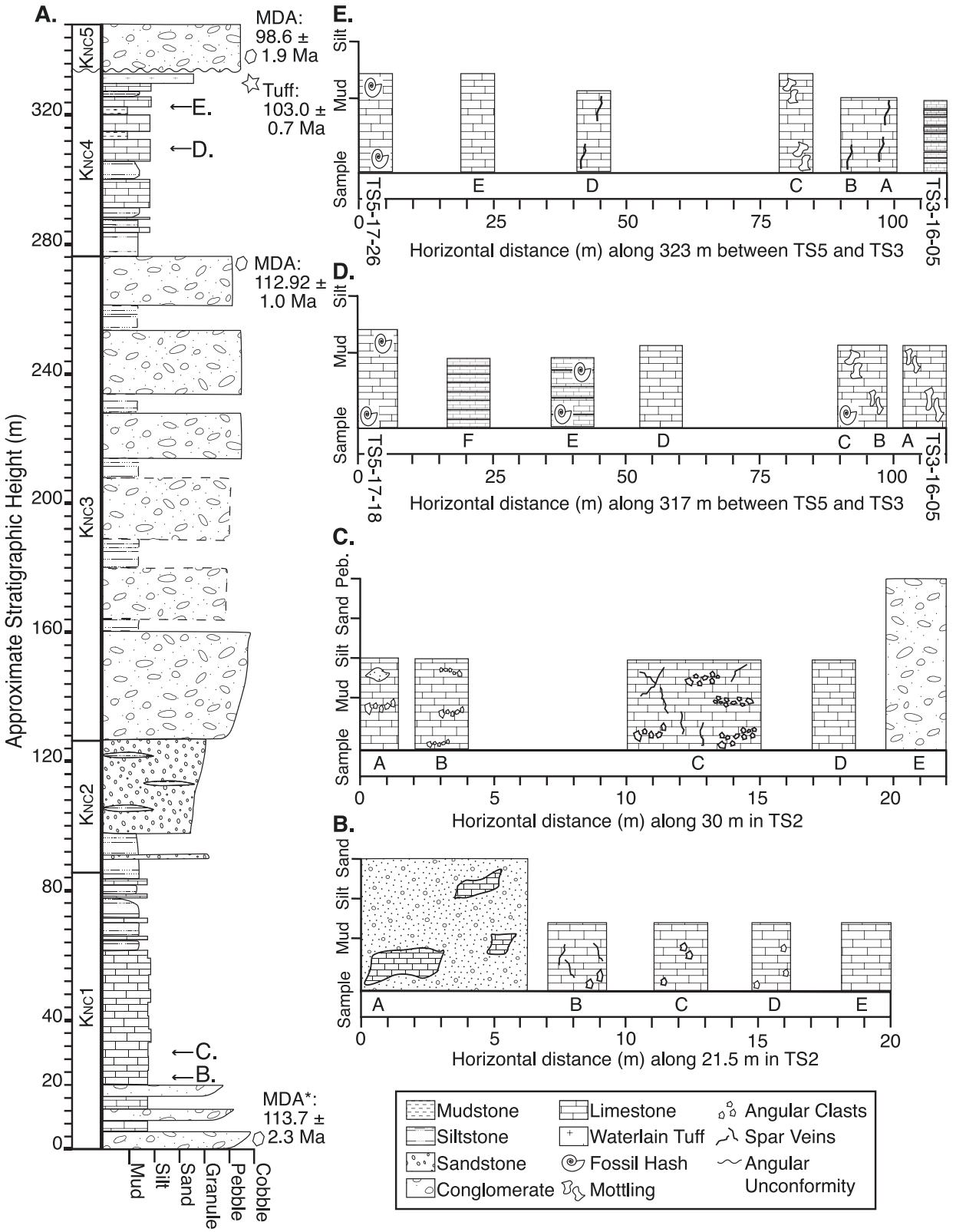

FIG. 3.—**A)** Composite stratigraphic column of the Newark Canyon Formation type section, in meters. The column integrates stratigraphic and lithologic information from the five measured sections to show general basin architecture. Note the angular unconformity between Knc4 and Knc5. U-Pb geochronologic age constraints showing a depositional age from a water-laid tuff (star) and three maximum depositional ages (MDA) from detrital zircons (hexagons) are shown to the right of the stratigraphic column (Di Fiori et al. 2020*)*. *Note: MDA used for base of the section was generated from basal mudstone sample located ~ 10 km north of the type section, in the Hildebrand exposure (west) of the Newark Canyon Formation. **B**–**E)** Lateral sections showing horizontal distance in meters and lithologic change along four stratigraphic heights: 21.5, 30, 317, and 323 m, respectively. Note the scale change in horizontal distance used for 21.5 and 30 m compared to 317 and 323 m.

TABLE 1.—*GPS coordinates for each measured stratigraphic section.*

Measured Section	Section Base		Section Top	
	Latitude (°)	Longitude (°)	Latitude (°)	Longitude (°)
TS2	39.51389	–115.85641	39.51727	–115.85650
TS3	39.52331	–115.85829	39.52151	–115.86955
TS4	39.52099	–115.86356	39.52062	–115.86467
TS5	39.52026	–115.86975	39.52051	–115.86988

(1959), which is a nongenetic classification system useful for providing description without assuming origin and are based on both hand-sample and thin-section analysis.

Additionally, we measured numerous short sections laterally at 21.5, 30, 317, and 323 m in the main section to assess lateral facies variability (Fig. 3). The lateral extents of these sections were determined by availability of exposure. Assessing the variability of facies laterally allows us to better understand the spatial scale and heterogeneity of facies changes on the landscape at a given depositional moment. In this context of spatial heterogeneity, we are better able to recognize vertical changes in sedimentation that are larger than the inherent spatial variability of the depositional systems.

We prepared a total of 85 thin sections for optical and cathodoluminescence microscopy to aid in facies analysis, fossil identification, and identification of diagenetic fabrics. Cathodoluminescence (CL) microscopy was conducted on a Technosyn Cathode Luminescence Model 8200 Mk II microscope. CL was used to identify primary depositional fabrics, diagenetic fabrics that resulted from dissolution and/or reprecipitation, recrystallization, and later void-filling cements. CL colors of carbonate minerals vary between yellow and orange to dull to nonluminescent according to the spatial distribution of trace elements (i.e., Fe, Mn) in carbonate fabrics and can be a visual aid in determining generations of crystallization through crosscutting relationships (Pagel et al. 2000). This technique has yielded useful information about primary and diagenetic components of carbonate facies that are similar to those preserved in the Newark Canyon Formation (Wright and Peeters 1989; Dunagan and Driese 1999; Mintz et al. 2011; Parrish et al. 2017).

RESULTS

We identified six distinct facies through assessment of both hand samples and thin sections and interpreted the corresponding environmental interpretations for each facies, in order of decreasing energy of the environment: 1) bedded conglomerate (Gb), 2) calcareous, clast-supported conglomerate (Gc), 3) planar-bedded sandstone (Sh), 4) mottled mudstone (Fm), 5) micrite (M), which includes the pebbly pelmicrite (Mp) and mottled micrite (Mm) subfacies, and 6) interbedded biomicrite and calcareous mudstone (Mb/Fc) (Table 2). The relationships between the facies defined here and the mappable members (Knc1–Knc5) laid out by Di Fiori et al. (2020) are shown in Figure 3.

Bedded Conglomerate (Gb)

Description: Field and Hand Sample.—The bedded conglomerate facies is characterized by massive to cross-bedded, pebble to cobble, clast-supported conglomerates. Beds range in thickness from 2 to 8 m and extend laterally between 50 to 200 m. Clasts are subangular to subrounded and are typically in a fine to medium sand matrix (Fig. 4A, C). Clasts are composed dominantly of red and black chert and gray quartzite. In the conglomerate beds, there are localized beds of horizontally laminated and trough cross-bedded medium sandstones. Sand lenses often show evidence of scour at the top (Fig. 4B, D).

Associated Facies.—The bedded conglomerate facies is commonly associated vertically with the planar-bedded sandstone (Sh) and mottled mudstone (Fm) facies.

Interpretation.—As previously interpreted by Vandervoort (1987), the characteristics of the bedded conglomerate (i.e., Vandervoort's upper conglomerate) are consistent with deposition by a high-energy, braided fluvial system with gravel bedloads. This interpretation is supported by the

TABLE 2.—*Lithofacies with associated facies, brief descriptions, and interpreted depositional setting.*

	Facies Name	Facies Code	Associated Facies	Facies Description	Depositional Interpretation
	Bedded conglomerate	Gb	Fm, Sh	Cross-bedded to massive, pebble to cobble clast-supported conglomerate. Interbedded with trough cross-bedded sandstones and poorly exposed siltstones.	Braided-river channels
	Calcareous clast-supported conglomerate	Gc	Mp, Mm	Crudely bedded, calcareous, clast-supported conglomerate. Clasts range from 0.5 mm to 3 cm. Includes numerous clasts of the pebbly pelmicrite. Channelforms are steep-sided, concave-up and laterally separated by $>$ 20 m.	Anastomosing-river channels
	Planar- bedded sandstone	Sh	Fm, Gb	Well-sorted, fine to medium quartz-rich sandstone. Planar-bedded with some very low-angle bedding.	Bars in a braided river system
	Mottled mudstone	Fm	Sh, Gb, Mp/Mm?	Dark gray to grayish brown, weakly lithified, massive mudstone. Crumbles into angular blocks that are on average 5 cm in diameter and has grayish-purple color mottling. Some carbonate nodules are sporadically present.	Interchannel areas of alluvial plain
Micrite (M)	Pebbly pelmicrite	Mp	Mm, Gc	Pale reddish brown peloid-rich micrite with siliciclastic sand- to pebble-size clast lenses composed dominantly of chert. Peloids ($\sim$ 100 μm to 1 mm) and have same grain size and texture as surrounding matrix.	Palustrine
Micrite (M)	Mottled micrite	Mm	Mp, Gc	Micrite with distinct, centimeter-scale mottling that varies from dark yellowish orange to moderate reddish brown. Some elongate cracks and voids are commonly partially spar-filled.	Shallow palustrine with prolonged subaerial exposure
	Interbedded biomicrite and calcareous mudstone	Mb/Fc		Interbedded fossiliferous (bivalve, ostracod, charophyte, and gastropod hash) micrite and calcareous siliciclastic mudstone. Beds range from 1 mm to 10 cm thick.	Lacustrine

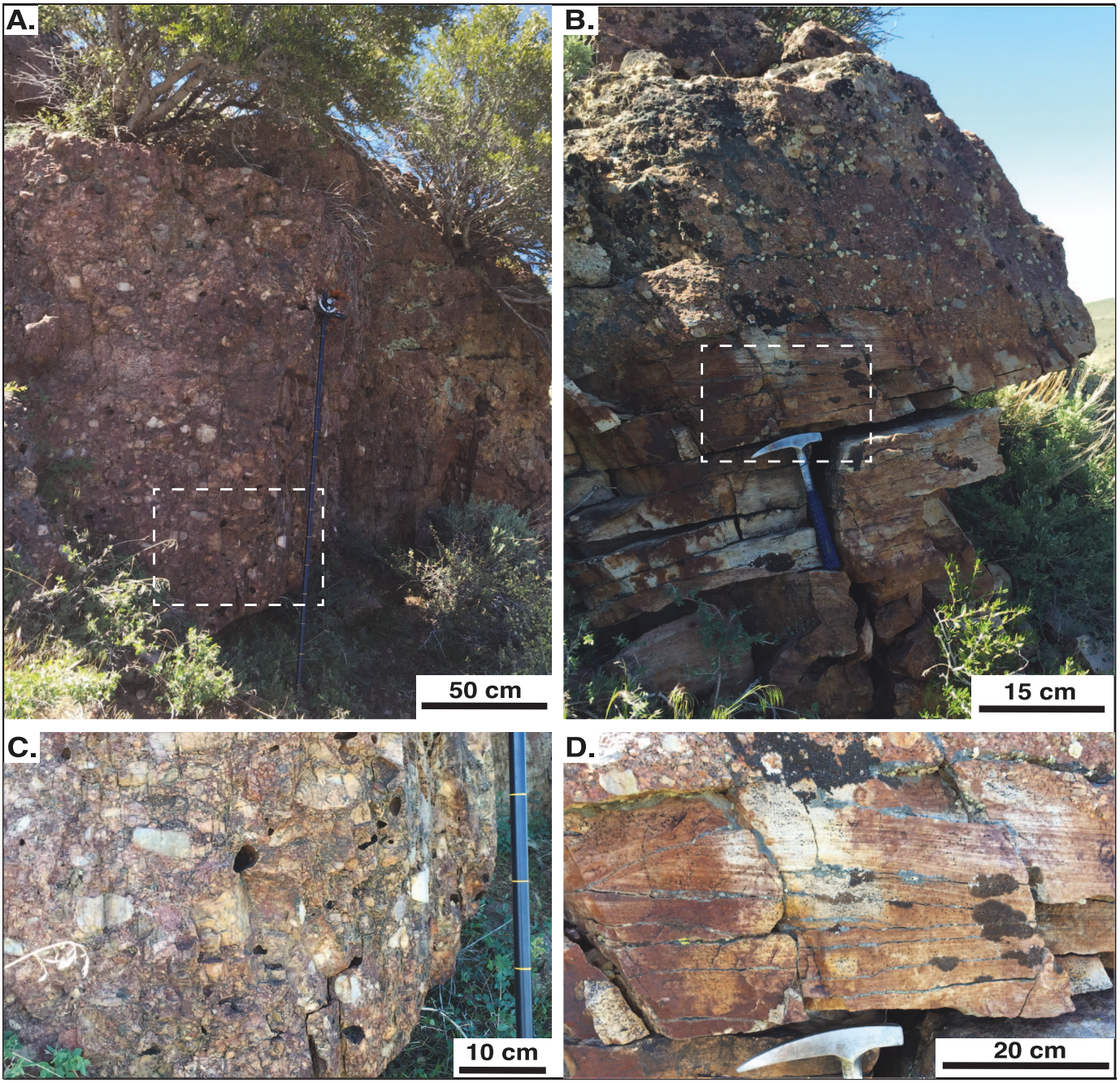

FIG. 4.—**A)** Outcrop photo of bedded conglomerate (Gb) facies. White box marks extent of photo shown in Part C. **B)** Outcrop photo highlighting a bed of cross-bedded sandstone in Gb facies. White box indicates extent of photo in Part D. **C)** Zoomed-in outcrop photo of Part A showing rounded, poorly sorted clasts composed dominantly of red and black chert, and gray quartzite. **D)** Zoomed-in outcrop photo of Part B. The top of localized beds of planar-laminated and trough cross-bedded, medium sandstones often show evidence of scour from conglomerates deposited on top.

abundance of coarse-grained material, scour features, and interbedding with the planar-bedded sandstone facies (Williams and Rust 1969; Rust 1972; Miall 1977a, 1977b). Additionally, the close association with the mottled mudstone facies suggests an abundance of fine-grained material, and therefore a fluvial system extremely choked with sediment (Miall 1977a).

Calcareous, Clast-Supported Conglomerate (Gc)

Description: Field and Hand Sample.—The calcareous, clast-supported facies is a poorly sorted, clast-supported pebble conglomerate with calcareous cement. This facies is generally massive with few internal structures, although some crude low-angle crossbedding was observed (Fig. 5A). No apparent clast imbrication was identified. Clasts are subrounded to subangular and are dominated by red and gray chert and gray limestone. There are notable clasts of pebble-rich, gray to red micrite similar to the pebbly pelmicrite facies (Fig. 5B, C). These micritic clasts are generally tabular, angular to subrounded, and range from 3 to 20 cm in length. The matrix is composed of medium, subrounded sand. Beds of the calcareous, clast-supported conglomerate occur in concave-up lenses that are no more than 5 m wide and 2 m thick.

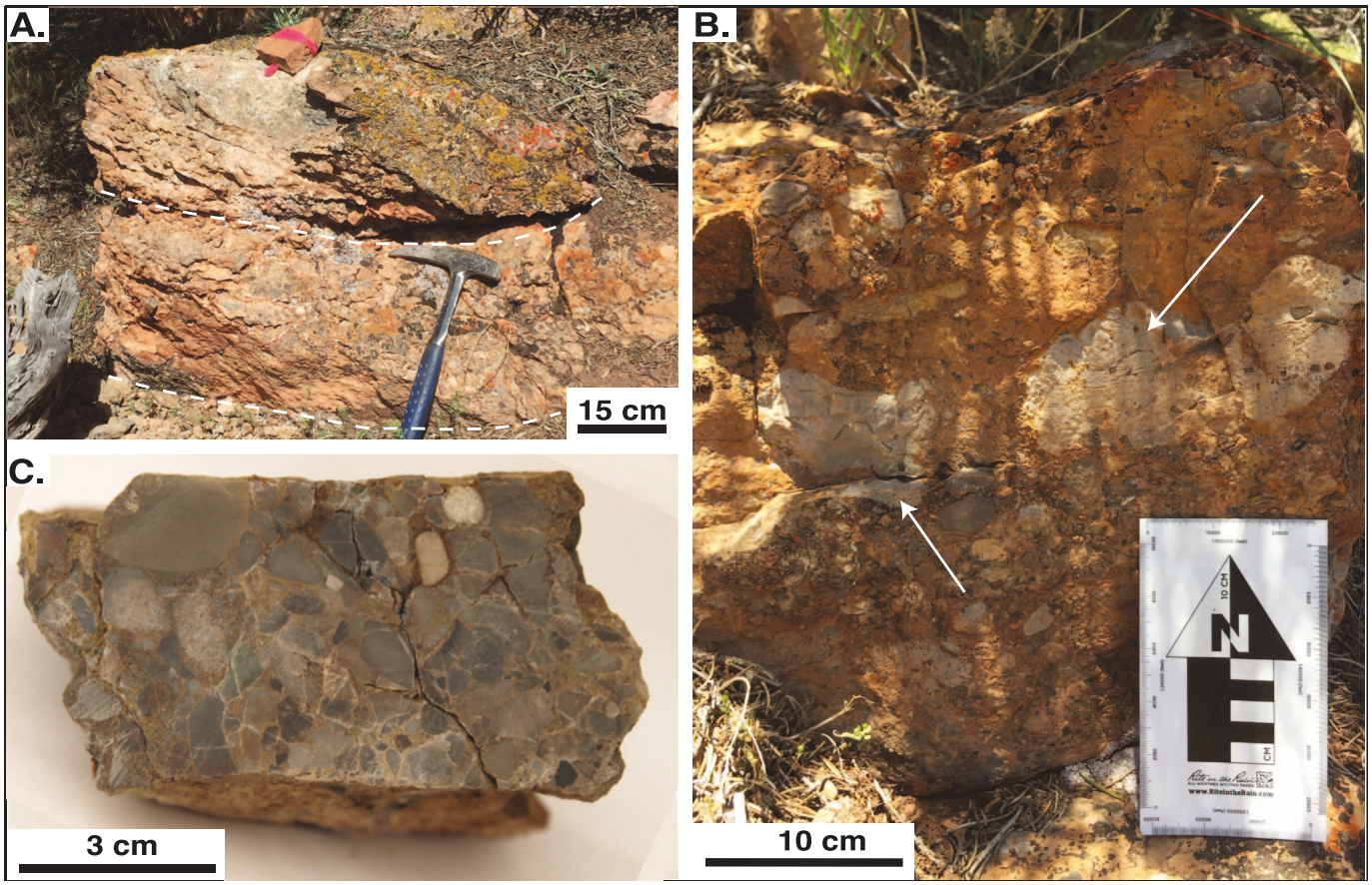

FIG. 5.—**A)** Outcrop photo of calcareous clast-supported conglomerate (Gc). White dashed lines trace concave-up channelforms. **B)** Outcrop photo of Gc with large rip-up clasts of gray micrite (white arrows). **C)** Polished hand sample photo of Gc.

Associated Facies.—Channelforms of the calcareous clast-supported conglomerate facies are consistently separated laterally by a minimum of 20 meters of the pebbly pelmicrite (Mp) facies. This conglomerate facies is bracketed vertically and horizontally by the pebbly pelmicrite (Mp) and mottled micrite (Mm) facies.

Interpretation.—We interpret the calcareous, clast-supported conglomerate to represent deposition in a fluvial system, likely an anastomosing river. Anastomosing river systems characteristically have spatially separated channels, high-angle channelforms, and close lateral association with fine-grained facies (Smith 1983, 1986; Nadon 1994). The accumulation of coarse-grained sediment in the channelforms indicates high vertical aggradation rates and a suspended-sediment system (Smith 1983; Makaske 2001). We interpret the angular clasts of micrite to be rip-up clasts that demonstrate reworking of previously deposited palustrine materials that were on the adjacent flood plains during periods of rapidly increased fluid flow. This kind of increased fluid flow could occur during the partial collapse of channel banks or channel avulsion (Makaske 2001). Transportation of the micrite clasts was likely brief due to the angularity and size of the rip-up clasts, which in some instances exceeded 20 cm in length. Desiccation of the interchannel areas was likely necessary in order for micritic rip-ups to survive transportation even a short distance during high-fluid-flow events (Lorenz and Gavin 1984).

Planar-Bedded Sandstone (Sh)

Description: Field and Hand Sample.—The planar-bedded sandstone facies is dominated by planar-bedded, well-sorted, fine to medium, quartz-rich sand. Grains are sub-rounded to rounded. Colors on a fresh outcrop surface range from pale red (5R3/2) to grayish orange (10YR7/4) (Fig. 6). The sandstone forms distinct 0.5 to 1 m beds, and individual beds tend to fine upwards. Some planar laminae and very low-angle cross laminae are locally present. No apparent scour forms were identified. Although partially hindered by the availability of exposure, we observed beds of this facies to be laterally continuous up to approximately 25 m. The Sh facies has local, calcite spar-filled fractures that typically range from 2 mm to 1 cm long.

Associated Facies.—The planar-bedded sandstone is commonly vertically associated with the mottled mudstone (Fm) and bedded conglomerate facies (Gb).

Interpretation.—We interpret the planar-bedded sandstone facies to represent deposition of sand bars in a braided river system. When water is forced across shallow bars in fluvial systems, fluid flows increase, causing low-turbulence, high-velocity flow regimes that form massive to horizontally laminated deposits of sand (Williams and Rust 1969; Miall 1977a). The kind of high fluid velocities that result in massive to horizontally laminated, well-sorted sands are often found in braided river systems (Miall 1977a; Martin and Turner 1999).

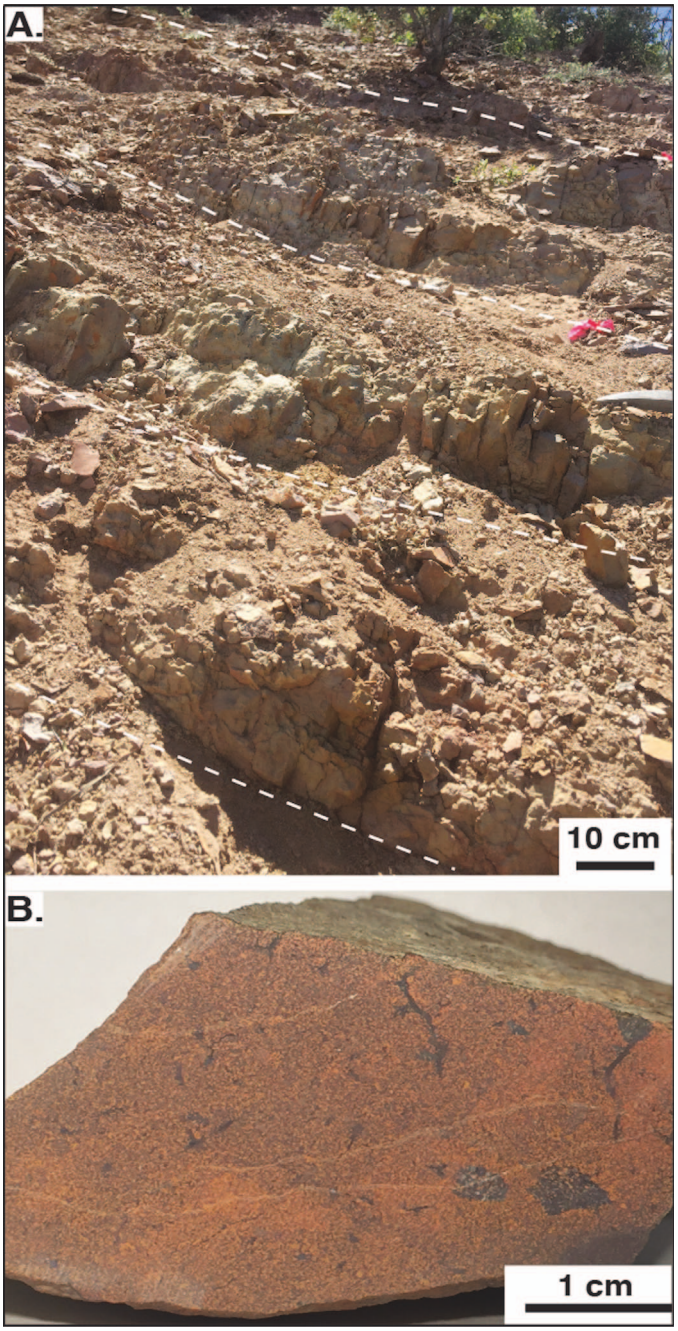

FIG. 6.—**A)** Outcrop photo of planar-bedded sandstone (Sh) facies. White dashed lines outline beds. **B)** Polished hand sample of massive sandstone facies. Dark lines throughout are spar-filled fractures.

Mottled Mudstone (Fm)

Description: Field and Hand Sample.—The mottled mudstone facies weathers recessively, resulting in limited exposure. The best exposure of this facies was found along a steep slope located south of the Newark Canyon Road (Fig. 2A, TS4). We trenched the approximately 20 m section and used it to characterize the facies. The mottled mudstone facies is composed of weakly lithified mud with fluctuating quantities of silt. Colors range between dark gray (N5) to grayish brown (5YR3/2) with grayish purple mottles (5P4/2) (Fig. 7A). Mottling is distinct and generally "coarse" (> 15 mm) in size. As shown in Figure 7A, this facies commonly disaggregates into angular blocks that average 5 cm in diameter. On the faces of some of these blocks, there is weak formation of visible slickensides. Carbonate nodules are present locally throughout the facies, though the nodules are not abundant. In addition, parts of the mottled mudstone facies have localized calcareous cement causing some horizons to be better lithified than others (Fig. 7B).

Associated Facies.—The mottled mudstone facies is associated with the planar-bedded sandstone (Sh) and bedded conglomerate (Gb) facies. Additionally, the mottled mudstone facies may interbed with the mottled micrite and pebbly pelmicrite facies, but poor exposure restricts our ability to test this possibility.

Interpretation.—We interpret the mottled mudstone facies as deposition of fine siliciclastic grains in the interchannel areas of an alluvial plain (Bown and Kraus 1987). The dominance of muds and silts in this facies indicates a low-energy regime. We interpret the consistently sized blocks into which this facies disaggregates as formation of subangular blocky peds caused by a network of irregular planes that create more stable aggregates of sediment (NRCS Soils Staff 2017). Slickensides, such as the ones identified on the faces of the peds, often form as a result of swelling clay minerals and shear failure during the development of the soil column (NRCS Soils Staff 2017). Characteristic soil structures, such as the presence of ped formation, slickensides, and carbonate nodules, suggest that some pedogenic development occurred in these sediments (Gray and Nickelson 1989; Mack et al. 1993; Kraus 1999).

Mottling signifies variable redox conditions that preferentially mobilized major cations (Duchaufour 1982). Variable redox conditions were likely caused by fluctuations in the height of the water table causing irregular wetting and drying throughout the sediment. The colors present in this facies are consistent with highly saturated, hydric soils (Richardson and Vepraskas 2001). Although carbonate nodules are typically not found in hydric soils due to unfavorable conditions for mineral precipitation, the limited presence of carbonate nodules in the mottled mudstone facies further supports wetting and drying cycles across the depositional landscape (Freytet and Plaziat 1982). The carbonate in this system was likely sourced from a combination of windblown sediment and dissolved carbonate in the pore water moving through the soil profile and the abundant primarily deposited carbonate throughout the type section. Dry-down periods would allow for the supersaturation of carbonate in the mudstone, thus creating conditions favorable for calcite precipitation.

Micrite to Microsparite (M)

The micrite facies consists of two subfacies: pebbly pelmicrite (Mp) and mottled micrite (Mm). While these two subfacies are the most common deposition types, there are instances where features from both commingle vertically and laterally and represent a gradation between these two endmembers. To highlight the subtle, yet important differences between the endmembers of this facies, the two subfacies are described and interpreted separately.

Pebbly Pelmicrite (Mp)

Description: Field and Hand Sample.—The pebbly pelmicrite facies is a peloid-rich, micritic limestone with local siliciclastic sand- to pebble-size clast lenses. The color of this facies ranges from pale reddish brown (10R5/4) to grayish brown (5YR3/2). In outcrop, exposed beds of the pebbly pelmicrite facies weather into rounded blocks and bedding thicknesses range between 0.25 m and 1.5 m (Fig. 8A). Pebble lenses are 2 cm to 10 cm thick and 5 cm to 1 m wide (Fig. 8B). Fine sand to pebble-sized clasts are composed of mixtures of gray and red chert, and

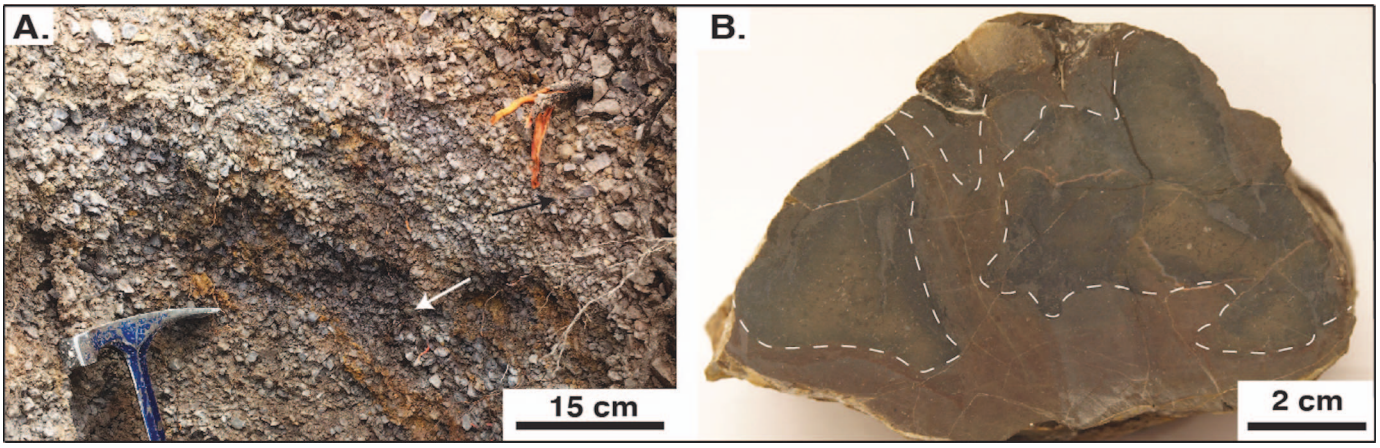

FIG. 7.—**A)** Outcrop photo of the mottled mudstone (Fm) facies. The white arrow highlights grayish-purple color mottling, and the black arrow points to the more abundant dark gray to grayish-brown color. Note the disaggregated angular blocks that average 5 cm in diameter. **B)** Photo of a carbonate nodule from Fm facies that shows centimeter-scale color mottling between grayish brown to dark gray color mottling (white dashed lines).

gray limestone. Clasts are typically angular to subrounded. A few large subangular to angular gray limestone clasts that range between 10 to 30 cm are locally suspended in the red micrite (Fig. 8A). Calcite spar is common as fracture fill.

Microscopy.—Petrographic analysis at 10 × magnification shows discrete, round peloids ranging in diameter between 100 μm and 1 mm that are evenly distributed in the micrite (Fig. 8C). Some types of peloids have a nucleus, such as a fecal pellet. Others do not and are classified as non-nucleated; the peloids in our samples fall into the latter category. The surrounding matrix and peloids are composed of the same grain size and texture. This is best demonstrated in the CL images of peloids where peloids all but disappear into the surrounding matrix (Fig. 8D, F). Peloids are evenly dispersed throughout the matrix and do not occur in distinct lenses or zones. Locally, peloids can encompass detrital grains. Additionally, the peloids commonly have an exterior rim of dense micrite (Fig. 8C, E). The crystal size of the matrix can vary between micrite and microsparite where microsparite matrix is typically found next to the spar-filled veins and grades to micrite within 200 to 500 μm from the vein (Fig. 8G, H). Additionally, thin rims of calcite spar that surround some pebbles and peloids radiate into the surrounding matrix (Fig. 8I, J). Root traces are present but not abundant. Where found, root traces range in width from 100 to 300 μm, are irregular in shape, commonly are perpendicular to bedding planes, and are filled with microspar and spar (Fig. 8K, L).

Associated Facies.—The pebbly pelmicrite facies grades laterally between the calcareous clast-supported conglomerate (Gc) and mottled micrite (Mm) facies within ~ 25 m.

Interpretation.—We interpret the micrite in the pebbly pelmicrite facies to be precipitation of carbonate mud from the water column as a result of supersaturation of calcium carbonate constituents (i.e., Ca^{2+} and CO_3^{2-}). A dense matrix with homogeneously sized micritic grains suggests an environment with low-energy levels that allowed fine-grained material to precipitate and settle out of the water column (Folk 1959). Although microspar can be a primary depositional texture, two features suggest that microsparite in this facies is largely a diagenetic texture that resulted from postdepositional recrystallization of primary micrite. One feature is the consistent localization of microsparite adjacent to spar veins (e.g., Lasemi and Sandberg 1993; Flügel 2004). Another feature is the CL characteristics of the micrite and microspar. Recrystallization is typically distinguished from other diagenetic fabrics by inconsistent CL color between micrite and coarser textures, and spatial gradation from finer to coarser crystals. Additionally, secondary precipitation of multiple generations of carbonate likely occurred in these deposits as indicated by the range of luminescence colors observed in the CL images, which often suggests multiple precipitation events from variable fluid sources (Fig. 8G–J) (Wright and Peeters 1989; Pagel et al. 2000).

The presence of peloids, consistent red coloring, and alteration rims around pebbles indicate that the pebbly pelmicrite facies experienced frequent, possibly seasonal, wetting and drying cycles. Peloid formation is common in environments that experience seasonal or episodic wetting and drying; the cycles can cause amalgamation and mild compaction of the matrix into spherical overprint features that are preserved as peloids (Wright and Platt 1995; Armenteros and Daley 1998). This process is often coupled with additional precipitation of micrite around peloid rims, creating semi- to fully coated peloid grains (Fig. 8E, F) (Alonso-Zarza and Wright 2010). Wetting and drying would also produce heterogeneity of sedimentary features on the centimeter- to micrometer-scale based on the abundance of clays in the carbonate matrix where more clay-rich zones will stay hydrated for longer (Alonso-Zarza et al. 1992). Additionally, red coloration typically results from an oxidizing environment with variable water level heights (Flügel 2004; Alonso-Zarza and Wright 2010). Therefore, based on the presence of peloids and red coloration, we argue that wetting and drying cycles are the most likely mechanism to create the peloids found in this facies. This interpretation is supported by the uniformity of texture, grain size, and CL color shared by the matrix and peloids, which indicates that peloids formed immediately after precipitation and deposition of the micrite (Freytet and Plaziat 1982; Armenteros and Daley 1998).

The root traces (Fig. 8K, L) preserved indicate some colonization of the micritic muds by vegetation (Alonso-Zarza et al. 1992). The limited abundance of root traces preserved in the Newark Canyon Formation suggests that establishment of extensive root systems was hindered in some capacity. This hindrance to vegetation was likely driven by a combination of rapid sedimentation rates, frequent inundation of the environment, and climatic factors, such as changes in mean annual and/or annual range of temperatures, or in the quantity and/or timing of rainfall.

We interpret the pebbly pelmicrite facies as formation of microcrystalline carbonate mud that precipitated out of solution in low-energy, spatially heterogeneous palustrine environments (i.e., wetlands). These shallow wetlands likely experienced variable periods of inundation and subaerial

exposure, establishment of vegetation, and intermittent pulses of sand- to pebble-size clasts (Wright and Platt 1995; Alonso-Zarza 2003).

Mottled Micrite (Mm)

Description: Field and Hand Sample.—The mottled micrite facies is composed of heterogeneous micrite that commonly has elongate cracks and spherical voids, and spar-lined veins that do not have a consistent orientation (Fig. 9). This facies is characterized by distinct centimeter-scale color mottling that varies between dark yellowish orange (10YR6/6) to moderate reddish brown (10R5/4) (Fig. 9A, B). The most visually distinct mottled regions typically are found surrounding spar-lined veins or voids.

Microscopy.—The majority of the thin sections show uniform micrite, though in areas surrounding dissolution and pull-apart voids, the micrite locally grades into calcite microsparite (Fig. 9E, F). Disconnected, amorphously shaped voids are found throughout the facies and range in size from 100 μm to 1 cm (Fig. 9G, H). Additionally, veins that range from 100 to 800 μm in length are present. Both the voids and veins are commonly lined with calcite and dolomite spar (Fig. 9G, H). Dolomite crystals (10 to 200 μm) are locally present in patches in the dense micritic matrix and are identified as dolomite due to their characteristic rhombohedral crystal shape and bright red cathodoluminescent color (Flügel 2004, p. 271). Rhombs typically disperse into the matrix from a densely concentrated area. Both dolomite and calcite crystals in veins and voids are present along the edges of the features and are rarely filled completely. Dolomite spar exhibits distinct color zoning in CL images (Fig. 9I, J). Siderite ($FeCO_3$) is present in a few zones (Fig. 9K, L). Siderite is identified based on its diagnostic tan to brown color, high surface relief, and low luminescent intensity indicative of abundant Fe^{2+}, a quenching cation (Pagel et al. 2000).

Associated Facies.—The mottled micrite facies grades laterally between the calcareous clast-supported conglomerate (Gc) and pebbly pelmicrite (Mp) within $\sim$ 25 m.

Interpretation.—We interpret the mottled micrite facies as deposition in a similar palustrine environment to that of the pebbly pelmicrite facies, although the mottled micrite likely experienced either longer periods of subaerial exposure or more rapid flooding and drying events (Freytet and Plaziat 1982; Freytet and Verrecchia 2002). This interpretation is based in part on the extensive pink and orange to gray mottling, which indicates strong variability in redox states that created irregular mobility of major cations such as iron (Fe^{2+}/Fe^{3+}) and manganese (Mn^{2+}/Mn^{3+}) at the centimeter-scale (Wright et al. 2000). Additionally, the presence of siderite in this facies demonstrates irregular concentrations of cations in the matrix, specifically Fe, which resulted in the deposition of the Fe-bearing carbonate minerals.

Further evidence of fluctuations between high-stand and low-stand periods is the presence of spar-lined cavities, which demonstrate changes in carbonate saturation stability causing uneven dissolution and then reprecipitation. We interpret most of these cavities to be desiccation cracks that resulted from drying and subsequent shrinkage of the micrite during subaerial exposure (Freytet and Plaziat 1982; Wright 1992; Wright et al. 1997). The irregular spar-lined veins and voids are likely the result of migration of fluids where surface tension holds the moisture to the walls of the pore space. This suggests precipitation of the void-lining secondary cement in the meniscus vadose zone (i.e., above the water table) (Flügel 2004). The absence of pebbles in the mottled micrite facies indicates that this facies either formed farther from the active channels that caused flooding and pulses of pebbles in the pebbly pelmicrite facies, or formed on slightly higher ground where only the largest flooding events could fully inundate the area. It is likely that both options are true for various exposures of the facies, which further supports the interpretation of a heterogeneous palustrine landscape that experienced variable inundation by water through time.

Interbedded Biomicrite and Calcareous Mudstone (Mb/Fc)

Description: Field and Hand Sample.—This facies consists of interbedded fossiliferous micrite and calcareous siliciclastic mudstone with abundant fossil hash. Beds of this facies are typically between 1 mm and 10 cm thick, which retain consistent thicknesses laterally along tens of meters (Fig. 10A). Where exposure allows, some outcrops of this facies can be traced laterally up to approximately 100 m. The biomicrite is medium gray (N5) to pale yellowish brown (10YR6/2) on fresh surfaces and exhibits no color mottling. The mudstone component of this facies varies between medium gray (N5) to moderate yellowish brown (10YR5/4) and commonly has a calcareous cement. Variable amounts of silt are present in this mudstone and intermittently there are discrete spheres of clay that range from 2 to 5 mm in diameter. Local dark, organic-rich partings are found in between laminae of mudstone and the biomicrite.

Microscopy.—Thin sections of this facies show dominantly micrite, with some local patches of microsparite that surround fossil fragments. Fossiliferous material is dominated by bivalve, ostracod, charophyte gyrogonites (i.e., calcified fructifications of Characeae), and gastropod fragments (Fig. 10). Silt-size detrital clasts are commonly dispersed throughout the dense micrite matrix. Silt clasts are dominated by chert and are subangular to subrounded. Cathodoluminescence images show that fossil fragments have undergone several stages of alteration that likely include dissolution and reprecipitation and multiple generations of void-filling cementation (Fig. 10C, D). Some fossil fragments have crystallized interiors of amorphous silica along with one to three generations of calcite precipitation (Fig. 10B–D).

Interpretation.—The fossiliferous micrite facies represents deposition in a lacustrine setting. The homogeneous nature of the micritic matrix of this facies suggests that carbonate precipitated out of the water column and settled at the bottom of the lake as a massive carbonate ooze. Additionally, the thin-bedded nature and lack of other sedimentary structures, such as ripples, as well as the extensive lateral continuity, indicates a low-energy regime, such as the deeper parts of a lake. Interbedding between the carbonate and mudstone beds suggests that conditions oscillated between periods when deposition of siliciclastic material or precipitation of carbonate was favored. The abundance of gastropod, ostracod, and bivalve fossil fragments and the lack of persistent organic preservation suggest that the lake was oxic (Tucker and Wright 1990; Flügel 2004). Additional evidence that the fossiliferous micrite facies was deposited in a low-energy, oxic lacustrine system is the presence of charophyte gyrogonites. Charophytes can reproduce both vegetatively and/or sexually, depending on species and environmental conditions such as water depth, temperatures, and salinity (García and Chivas 2006; Soulié-Märsche and García 2015). The presence of gyrogonites demonstrates that charophytes in this system were reproducing sexually, which is more common in persistent and shallow lakes with high water alkalinity (García and Chivas 2006; Sanjuan and Martín-Closas 2012).

DISCUSSION

Depositional Models

Stage 1: Anastomosing River with Interchannel Palustrine Environments

The base of the type section of the Newark Canyon Formation is characterized by palustrine carbonates interbedded with crudely bedded,

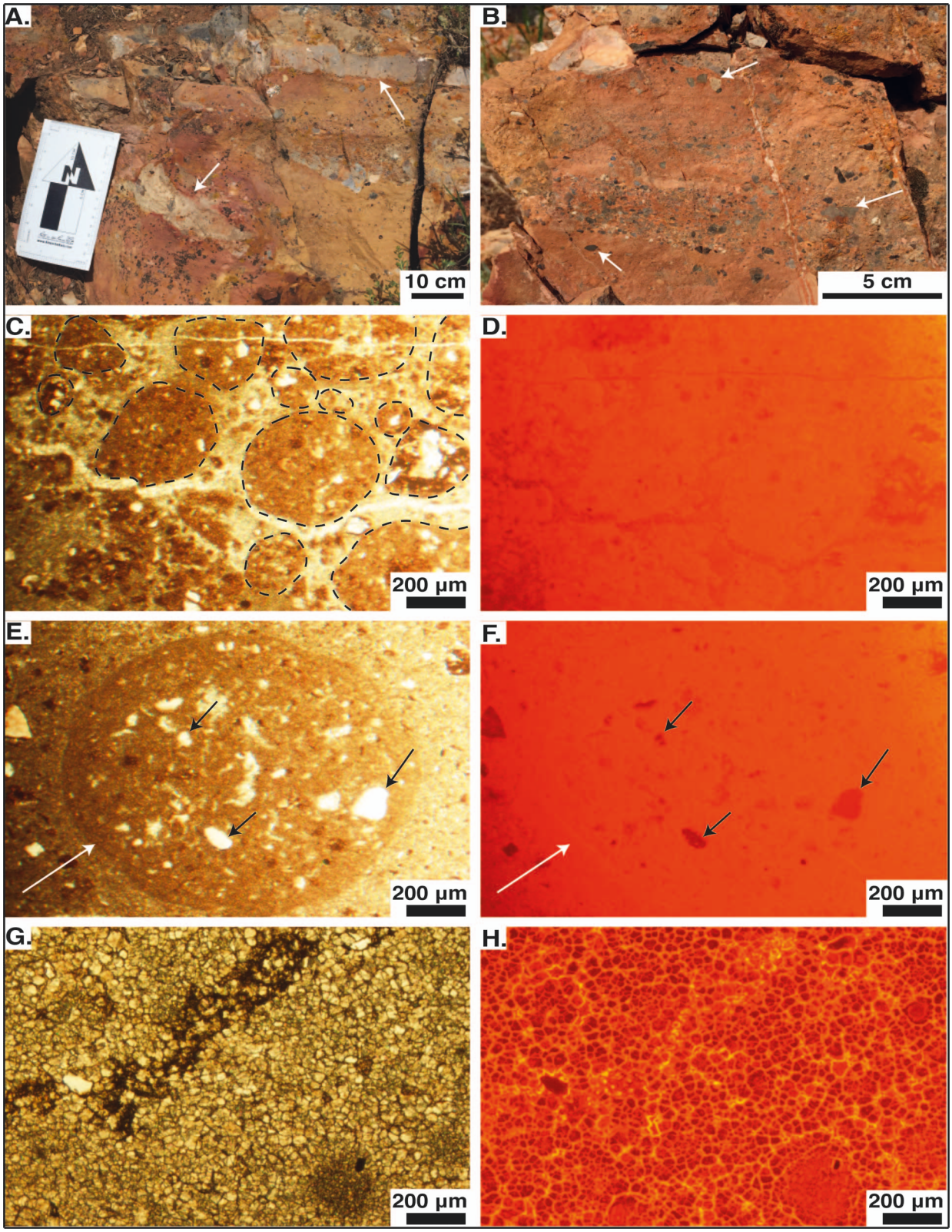

FIG. 8.—Outcrop and thin-section images of the pebbly pelmicrite (Mp) facies. **A)** Outcrop photo of Mp at approximately 16 m from the base of section TS2. White arrows highlight large, subangular to angular gray limestone rip-up clasts. **B)** Outcrop photo of Mp at approximately 19 m from the base of section TS2. Lenses of chert and limestone pebbles fine upwards in the dense reddish micrite. White arrows indicate examples of angular clasts. **C)** Plane-polarized-light (PPL) photo showing a cluster of subrounded to rounded peloids, indicated by black dashed lines, that range in size between 100 and 500 µm. **D)** Corresponding cathodoluminescence (CL) photo to Part C. The peloids and the surrounding matrix are interpreted as the same generation of micritic deposition based on the similarity of color between the interior of the peloids and the surrounding matrix. **E)** PPL photo of large peloid. The black arrows point to detrital grains in the peloid. The white arrow points to the dense micritic rim around the peloid. **F)** Corresponding CL image of Part E with arrows pointing to detrital grains as in Part E. The large peloid appears indistinguishable from the surrounding matrix based on luminescence colors and is highlighted by the white arrow positioned in the same place as Part E. **G)** PPL image of microsparite diagenetic fabrics interpreted to be associated with secondary precipitation of multiple generations of carbonate. **H)** CL image corresponding to Part G that shows dissolution and/or reprecipitation rims (bright yellow) separating primary material (darker, less luminescent red).

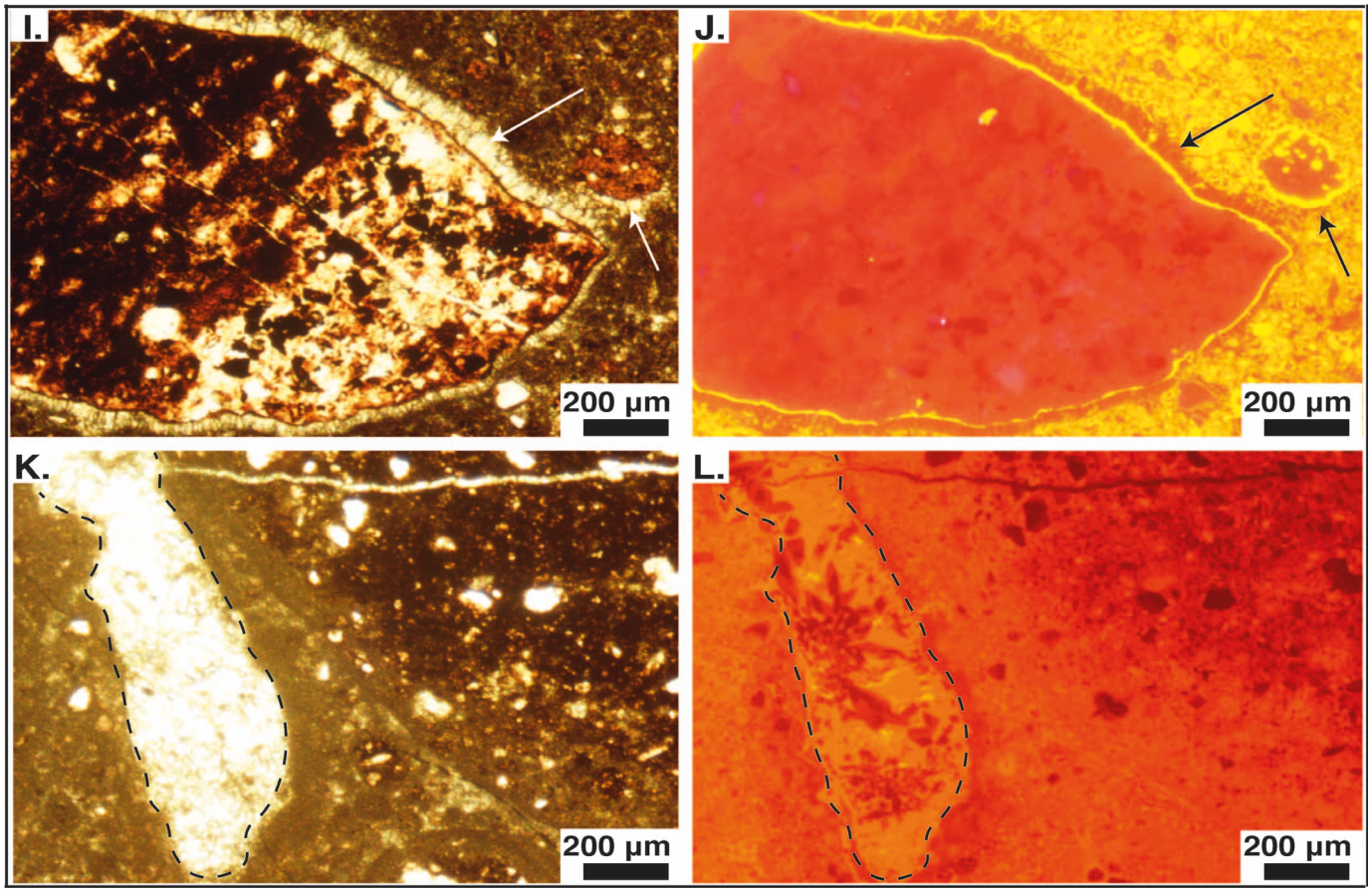

FIG. 8.—**I)** PPL image of subangular pebbles with rims of calcite spar (white arrows). **J)** Corresponding CL image of Part I that shows multiple generations of carbonate precipitation that range from reddish-pink to bright yellow. **K)** PPL image of Mp micrite with dispersed spar crystals and a preserved root trace (delineated by a black dashed line) with calcite fill. **L)** Corresponding CL image of Part K that shows at least two generations of calcite in-fill in the root trace: a dull yellow and a dark red. Note that the micrite matrix nearest to the root trace is a lighter orange than the darker red micrite farther away. This could be due to minor changes in the abundances and oxidation states of Fe and Mn surrounding the root due to perturbation of the matrix and changes in fluids movement into and through the matrix.

channelized, and laterally discontinuous conglomerate beds. The presence of conglomerates requires a depositional setting in which there are intermittent periods of fluvial deposition with energy high enough to transport pebble- to granule-size material. Shallow, low-energy environments must have been able to develop near the conglomerate channels in order to develop the associated palustrine carbonate facies. Braided, meandering, and anastomosing river systems all could fit these broad criteria. We argue, however, that an anastomosing system best fits Stage 1 of the Newark Canyon Formation, for a number of reasons. First, braided rivers are characterized by deposition of coarse material (sand to cobble) in multiple broad, shallow channels that shift rapidly, and form point and linguoid depositional bars (Miall 1977a, 1977b). The apparent lack of broad, fining-upward conglomerate sequences and the overall dominance of fine-grained material in the basal part of the type section argues against a braided river. Second, and in contrast to braided systems, meandering river systems have a single dominant channel with point bars in the concave sides of meanders and overbank deposits during floods that cause vertical accretion on the floodplain (Allen 1970; Miall 1977a, 1977b). The lack of point-bar and meanderloop deposits in the base of the section and the presence of multiple channelforms preserved within $\sim$ 25 m of one another provides evidence against a meandering river system as the depositional setting for the base of the type section. While we have interpreted the base of the type section as an anastomosing system, without more lateral exposure we cannot rule out that the system was instead an avulsion-prone, single-channel fluvial system. Both produce similar facies assemblages but could be distinguished by the presence of multiple coeval active channels that are characteristic of anastomosing systems.

Anastomosing rivers, as defined by Nadon (1994), are suspended-load systems composed of multiple interconnected, steep-sided, sand-bed channels that are confined by prominent levees and are separated by interchannel topographic lows. Topographic lows develop between channels because of vertical aggradation and development of distinct levees made of cohesive fine-grained material, such as calcareous muds (Nadon 1994; Makaske 2001). These levees create a characteristic inversion of the typical floodplain geometry where, in contrast to systems with an incised river channel and elevated floodplain zones, the interchannel areas are topographically lower than the levee-contained channels. In these topographic lows, significant crevasse-splay, lacustrine, and palustrine deposition can occur (Smith and Smith 1980; Smith 1986; Nanson and Croke 1992) and can constitute between 60 and 90% of anastomosing river deposits (Smith 1983; Nadon 1994; Makaske 2001). Additionally, anastomosing systems are characterized by highly variable fluid flow regimes which result in frequent lateral facies shifts and generally complex vertical arrangements of facies (Arenas-Abad et al. 2010). Frequent flooding events or channel avulsions are common in anastomosing systems (Makaske 2000). Pebble lenses record sporadic periods of high-energy flow likely due to brief flood pulses inundating the wetland systems from higher-energy adjacent channels. Additionally, flood

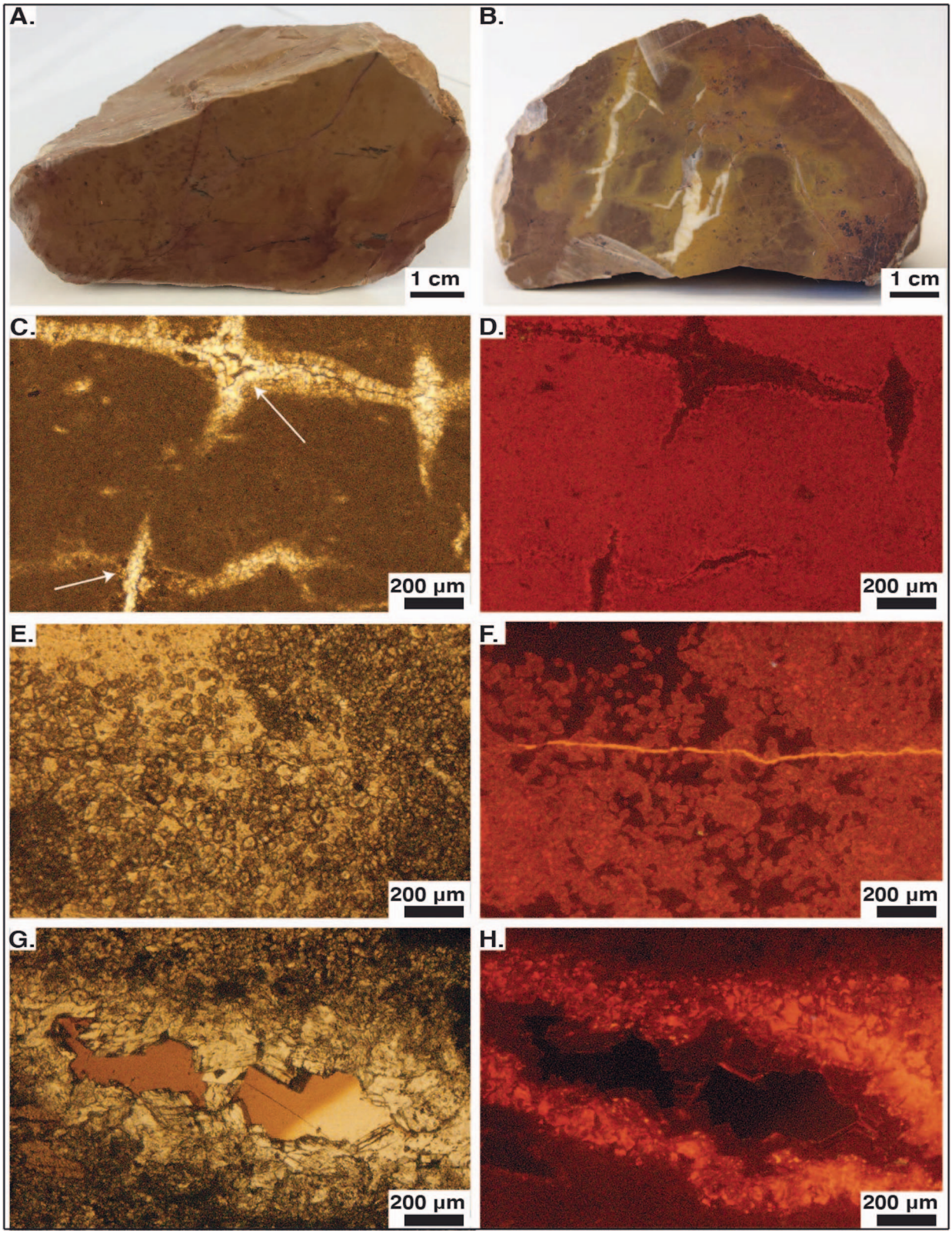

FIG. 9.—Outcrop and thin-section images of the mottled micrite (Mm) facies. **A)** Hand sample of Mm highlighting subtle light tan to pink to red mottling. **B)** Hand sample of Mm that shows distinct mottling from dark red to dark yellow brown and spar-filled desiccation cracks. **C)** Plane-polarized-light (PPL) image of dense micrite with several pull-away fractures (white arrows) with calcite spar lining the voids. **D)** Corresponding CL image of Part C showing homogeneous micrite and the clear difference in color between the matrix and spar lining. **E)** PPL image of calcite microsparite that grades into micrite. **F)** Corresponding CL image of Part E. Microsparite has a brighter luminescence than the micrite, while a crosscutting vein is a distinctly brighter yellow, demonstrating three generations of calcite precipitation. **G)** PPL image of a large void in the Mm facies with lining of spar. **H)** Corresponding CL image of Part G that shows a halo of bright luminescence surrounding the void space.

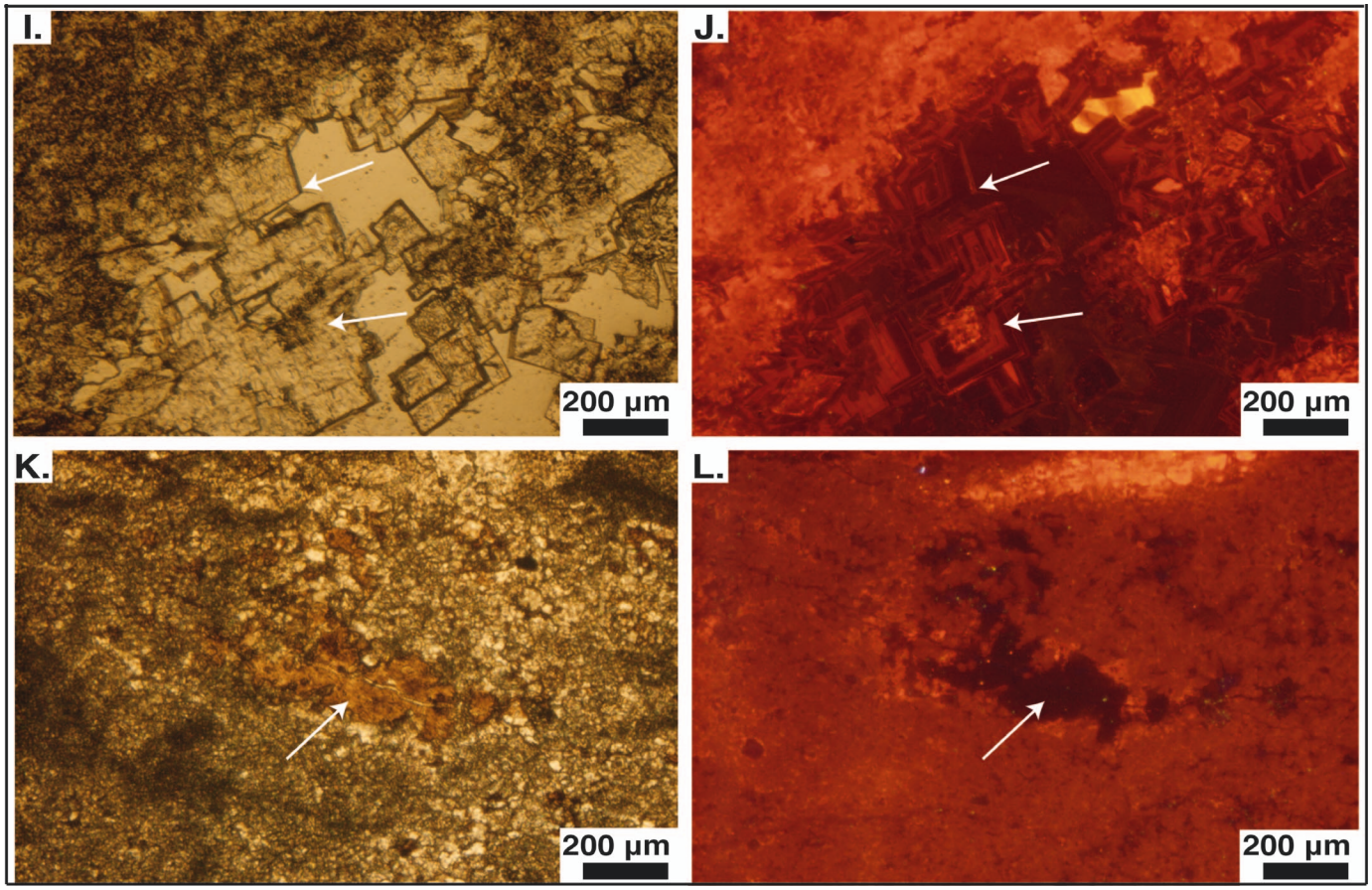

FIG. 9.—**I)** PPL image with examples of the dolomite spar, indicated by white arrows, present locally throughout the Mm faces. **J)** Corresponding CL image of Part I that highlights the dark red to red zoning in dolomite. **K)** PPL image of siderite (white arrow) that we interpret to be secondary precipitation that filled pore space within Mm due to the amorphous fill pattern. **L)** Corresponding CL image to Part K demonstrating the quenching nature of siderite and resulting dark CL color (white arrow).

pulses can rip up and locally redeposit material recently deposited in interchannel areas (Lorenz and Gavin 1984). The complex interbedding of the pebbly pelmicrite, mottled micrite, and the calcareous conglomerate, as well as the presence of rip-up clasts and pebble lenses in the pebbly pelmicrite facies, are consistent with the kind of highly variable fluid-flow regime found in anastomosing systems (Fig. 11). This agrees with the analysis put forward by Vandervoort (1987) and provides additional lines of evidence to support this interpretation via extensive assessment of the fine-grained carbonate that dominates the section.

We interpret the interchannel regions between anastomosing river channels as seasonally ephemeral palustrine, or wetland, environments. Palustrine environments are defined as the transitional zone between subaqueous and subaerial settings. This transitional zone can be both spatial (e.g., between lacustrine and pedogenic regions) or temporal (i.e., the transition that occurs due to periodic wetting and drying cycles). At the core of the definition of palustrine carbonate is the relationship between primary deposition, which is typically considered to be the result of processes similar to those in a shallow lacustrine or very slow moving fluvial setting, and the immediate diagenesis of that carbonate as a result of subaerial exposure and additional alteration by biotic and pedogenic processes (Platt 1989; Wright et al. 2000; Alonso-Zarza and Dorado-Valiño 2006; Marty and Meyer 2006; Murru et al. 2015). Alonso-Zarza (2003) lays out a comprehensive, carbonate-oriented depositional model that highlights the spectrum of carbonates that commonly form in palustrine environments. These features include extensive color mottling resulting from variation in redox states throughout the matrix, brecciation of the matrix due to wetting and drying cycles, creation of grains such as peloids from the primary matrix due to the coalescence of matrix material that occurs because of uneven contraction during drying, calcification of root traces, and other bioturbation evidence (Fig. 11) (Alonso-Zarza 2003). We observe all of these features in Stage 1 of the Newark Canyon Formation.

There are a few common palustrine sedimentary structures that are notably absent from the Newark Canyon Formation, such as pseudo-microkarst structures and rhizocretionary calcretes. The absence of these features provides further insight into the depositional setting of Stage 1 of the Newark Canyon Formation. Both pseudo-microkarst fabrics and rhizogenic calcretes are associated with roots systems and are often used to identify depositional stages where there were established vegetative communities on the landscape (Klappa 1980; Freytet and Plaziat 1982; Wright 1989; Jaillard et al. 1991; Wright et al. 1995; Freytet and Verrecchia 2002; Alonso-Zarza and Wright 2010). Pseudo-microkarst structures form through the mechanical enlargement of voids in the sediment, such as those that develop from a complex network of root traces, that are then infilled with multiple phases of sediments and cements (Freytet and Plaziat 1982; Alonso-Zarza et al. 1992; Freytet and Verrecchia 2002; Marty and Meyer 2006; Alonso-Zarza and Wright 2010). Rhizocretionary calcretes are typically interpreted as calcified root mats that can develop in indurated surfaces, such as in lacustrine and palustrine environments, or hardpans (i.e., petrocalcic horizons) on stable surfaces

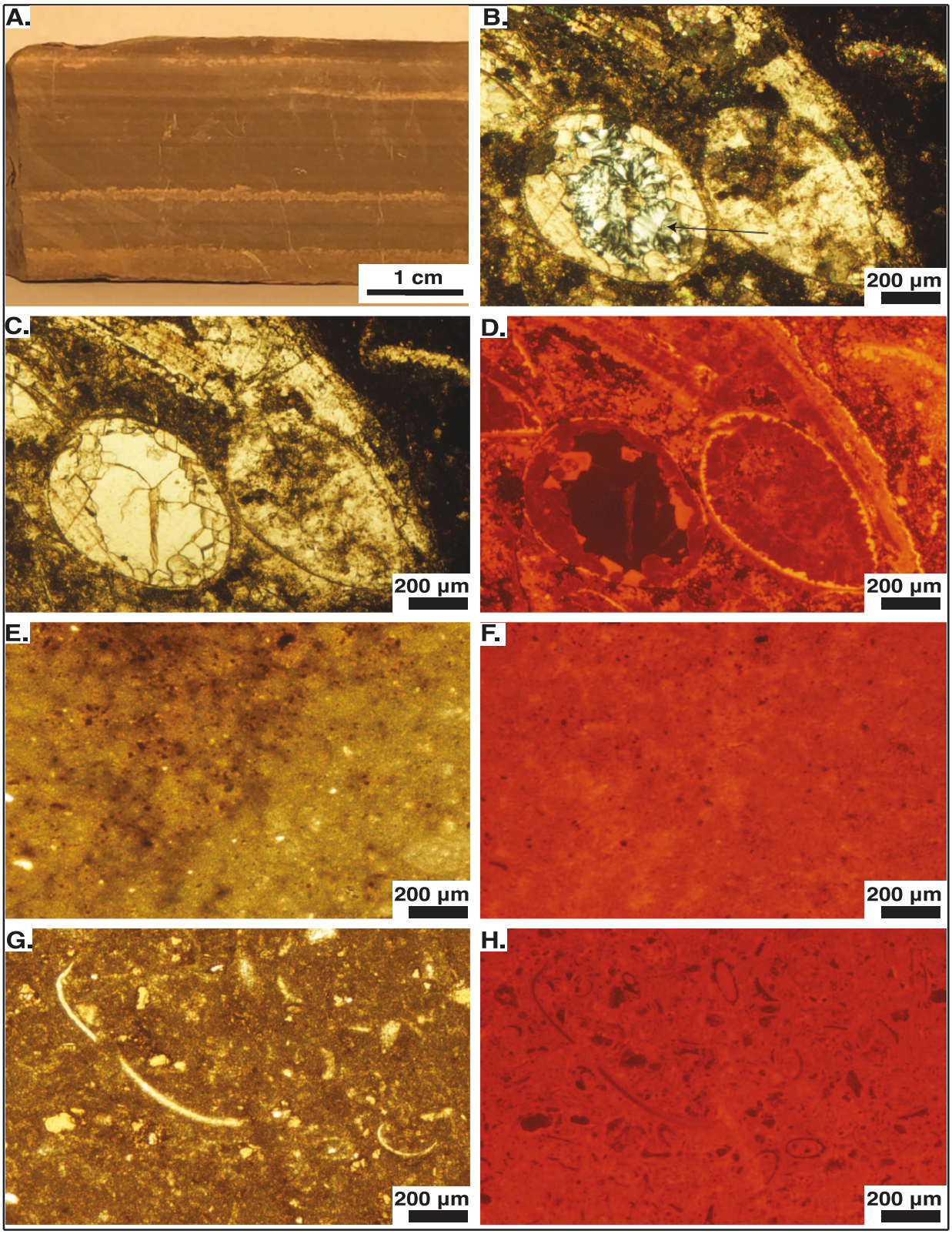

FIG. 10.—Outcrop and thin-section images of the interbedded biomicrite and calcareous mudstone (Mb/Fc) facies. **A)** Hand-sample photo of the Mb/Fc facies showing millimeter-scale interbedding between tan to light brown carbonate and medium-brown mudstone. This is an example of the thinner-bedded endmember of this facies. **B)** Cross-polarized light (XL) of ostracod and bivalve fragments that highlights the multiple generations of crystallization preserved. The white arrow points to silica crystals surrounded by calcite spar. **C)** Corresponding plane-polar light (PPL) image of Part B that shows a dense micrite matrix surrounding the fossil fragments. **D)** Corresponding CL image of Parts B and C that shows at least three generations of carbonate precipitation and the highly quenched silica that fills one of the ostracod fossils. **E)** PPL image of

(Klappa 1980; Wright 1989; Jaillard et al. 1991; Wright et al. 1995). The absence of well-developed pseudo-microkarst and rhizogenic calcretes in the pebbly pelmicrite and mottled micrite facies indicates a lack of the establishment of an extensive root system on the landscape, which is consistent with the relatively low abundance of root traces seen in the pebbly, pelmicrite and mottled micrite facies. As discussed above, this absence was likely caused by rapid sedimentation rates and frequent avulsion events of the anastomosing channels during Stage 1.

Another useful classification system for characterizing drivers of sedimentation during Stage 1 is the classification of terrestrial lake-basin systems proposed by Carroll and Bohacs (1999). Sedimentation during Stage 1 of the Newark Canyon Formation is considered to represent an over-filled basin type which is characterized by fluvial to shallow lacustrine facies associations that typically have distinct lateral facies changes and extensive fluvial input (Carroll and Bohacs 1999; Bohacs et al. 2000). In this system, the interchannel palustrine environments would have experienced variable amounts of subaerial exposure. Periods of flooding would have inundated the palustrine environments with subsequent dry-downs as the water level fell (Lorenz and Gavin 1984; Makaske 2001; Nadon 1994; Alonso-Zarza 2003). The length of time required for a palustrine environment to transition from subaqueous to subaerial conditions may be quite short (Wright and Platt 1995; Alonso-Zarza 2003; Alonso-Zarza and Wright 2010). Dry-downs can occur across a wide range of timeframes that can span from weeks, such as the periods between episodic storms, to months, for example a region that warms after a flooding season, or to years with the drop of regional base level. We conclude that dry-downs during Stage 1 of the Newark Canyon Formation ranged between seasonal to subseasonal (months to year) cycles and represent relatively rapid fluctuations in water levels due to the short-length-scale heterogeneity found in the complex spectrum of the palustrine facies observed.

The pervasiveness of carbonate facies in Stage 1, as well as throughout the whole Newark Canyon Formation, was likely facilitated by the underlying Permian Carbon Ridge Formation and Carboniferous Ely Limestone units contributing detrital carbonate and/or dissolved constituents into the regional hydrologic system. Additionally, these units contain interbeds of chert-rich conglomerates which likely contributed the reworked chert clasts into Stage 1 of the Newark Canyon Formation (Nolan et al. 1956; Roberts et al. 1967). The clasts of gray limestone found in the pebbly, pelmicrite facies are likely fragments of either the underlying Permian Carbon Ridge Formation or Carboniferous Ely Limestone based on the similarity of color and the distinct rough weathering texture.

Stage 2: Braided River

Previous interpretations by Vandervoort (1987) invoke a meandering-river setting for the massive sandstone and mottled mudstone facies, and then an abrupt shift to a braided river to deposit the conglomerates in the middle of the section. However, a few key features of a meandering system are missing, such as obvious channel fills with point-bar sedimentation (Miall 1977a; Smith 1987). We argue that a braided river system, however, could deposit the whole heterogeneous assemblage of facies found in Stage 2 of the Newark Canyon Formation type section (Fig. 11). In particular, the Donjek-type braided river characteristically has fining-upward cycles and an abundance of sand- and silt-dominated bars and overbank deposits (Miall 1977b). In the rock record, Donjek-type braided rivers commonly are identified as basin-filling sequences where cyclical packages range between 3 to 60 m thick and have notable lateral variation within the coarser-grained facies (Williams and Rust 1969; Miall 1977a, 1977b). Gravelly conglomerate facies can lack internal structures when the ratio of pebbles to sand is high, and commonly have shallow channels of cross-bedded sandstones similar to bedding observed in the bedded conglomerate facies in Stage 2 of the type section (Fig. 11). While poor exposure in the type section hinders definitive identification of cyclical deposition, the repeated exposure of conglomerate beds regularly spaced between recessive, slope-forming materials throughout the section is suggestive of the characteristic cyclicity of the Donjek-type braided river. Close vertical association of the bedded conglomerate, massive sandstone, and mottled mudstone found in TS4, as well as localized and discontinuous outcrops of sandstone and mudstone observed in TS3 suggest that the mottled mudstone and massive sandstone represent the fine-grained facies in the Donjek-type depositional cycle.

Stage 3: Lacustrine Environment

We agree with the interpretation of Vandervoort (1987) that the basin developed into a freshwater lake during Stage 3 of the type section, based on evidence for a continuously subaqueous and lower-energy environment (Fig. 11). Although we were limited by available exposure when assessing the approximate extent of the lake, lateral sampling along two stratigraphic levels near the top of the section provide a minimum estimate of 110 m of continuous lacustrine deposition (Fig. 3). We found no facies indicative of deposition along a shoreline, and therefore the estimate above represents a particularly conservative value for the spatial extent of the paleolake. Water height estimations are difficult, but we suggest that the lake was likely tens of meters deep. The continuity of sedimentation indicates that deposition of both the micritic and mudstone component of the lacustrine facies was the result of suspension settling of material out of the water column.

Using the lacustrine classification system proposed by Carroll and Bohacs (1999), we interpret the lacustrine setting in Stage 3 of the Newark Canyon Formation to be a balance-filled basin with fluctuating profundal facies. Balance-filled systems are characterized by laterally continuous sedimentation and variable fluvial input of siliciclastics into the basin, which would allow for the alternating siliciclastic- and carbonate-dominated sedimentation preserved (Carroll and Bohacs 1999; Bohacs et al. 2000). Additionally, the lack of evaporitic mineral deposits, such as gypsum or halite, indicates that the lacustrine system was not an underfilled basin. Semi-regular fluctuations in the balance between siliciclastic input and carbonate saturation is needed to create the interbedded biomicrite and calcareous mudstone. We infer that both siliciclastic settling and inorganic carbonate precipitation occurred at the same time in this basin, although during parts of the year the carbonate precipitation increased substantially, causing a dominance of carbonate sedimentation during those times of the year.

It is important to acknowledge that siliciclastic input into the basin and carbonate production in the basin could be coupled, where both sedimentation styles increase at the same time due to changing environmental conditions. For example, periods of increased precipitation with a subsequent dry-down period, such as monsoon-driven summertime rainfall events followed by drier periods, would likely deliver pulses of terrigenous sediment into the lake basin while also contributing to an increase in concentrations of major cations and anions (e.g., $[Ca^{2+}]$ and $[CO_3^{2-}]$, respectively) that could cause an increase in carbonate saturation. Conversely, the two sedimentation types could be uncoupled, and it is

←

dense micrite. **F)** Corresponding CL image of Part E showing homogeneous luminescence across micrite. **G)** Invertebrate fossil hash, including bivalve and ostracod fragments, supported by a dense micrite matrix. **H)** Corresponding CL image of Part G showing homogeneous luminescence across the micrite. Note the similarity in luminescence color between the micrite in Parts H and F.

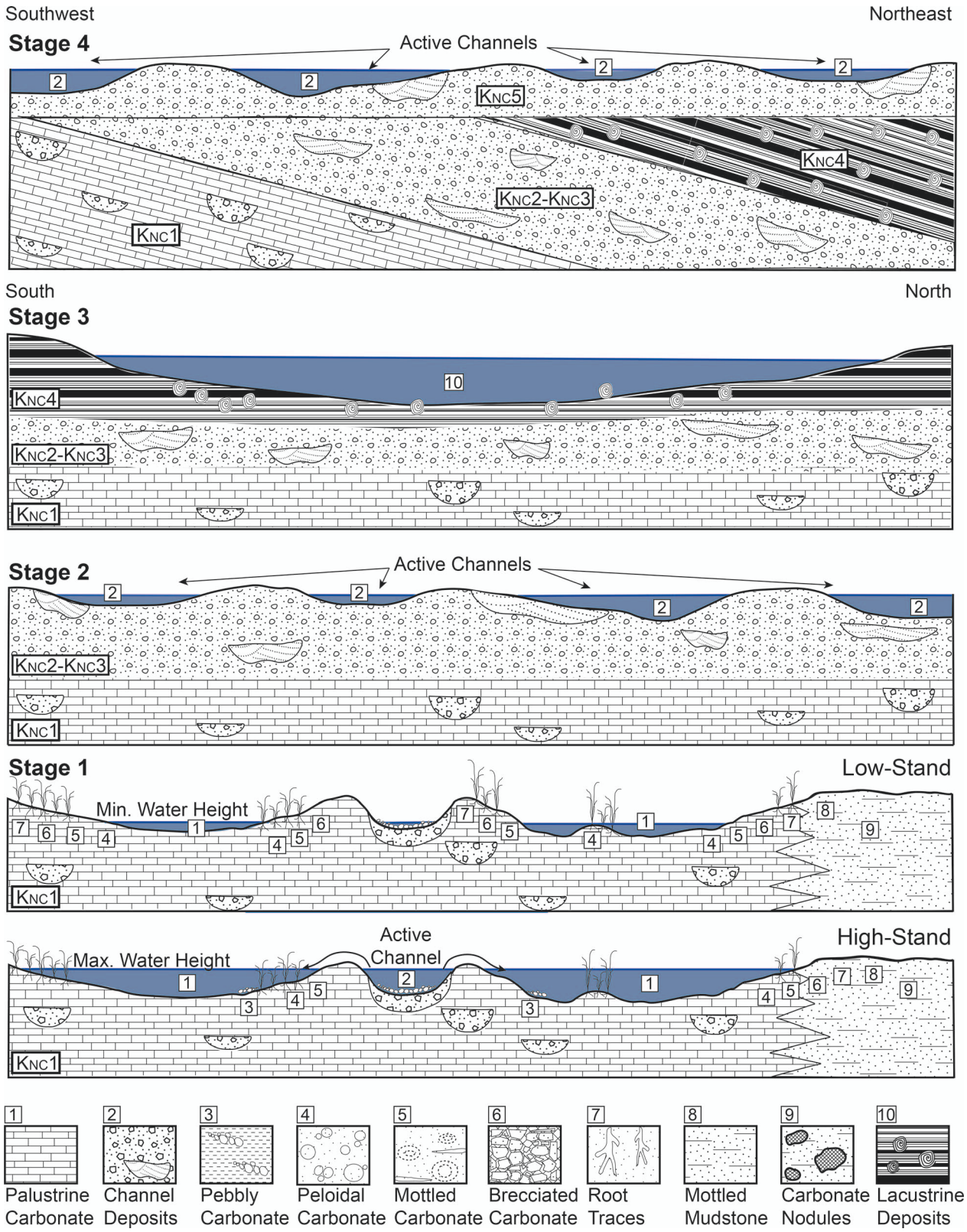

FIG. 11.—Generalized deposystem cross sections that represent the main depositional stages of the type section of the Newark Canyon Formation. Key depositional features and where they typically occur on the landscape are shown, indicated by numbers 1–10. Palustrine carbonate sedimentary features follow the facies model developed by Alonso-Zarza et al. (2003). Sedimentary features are not to scale, and horizontal and vertical scales vary between stages. Mappable unit (Knc1–5) labels and corresponding maximum depositional ages follow Di Fiori et al. (2020). Blue lines indicate the average water height on the landscape except when otherwise specified. **Stage 1:** Anastomosing river system with interspersed palustrine environments that correspond to Knc1. The maximum water height (~ 2–3 m) and minimum water height (> 1 m) of

possible for that same increase in precipitation to increase terrigenous input while causing a high-stand in the lake level that would decrease carbonate saturation. This question is outside the scope of this study but will be addressed in later work using traditional single and clumped stable isotopes to understand aspects of basin hydrology and influences on carbonate saturation.

Stage 4: Capping Braided River

We interpret Stage 4 of deposition in the Newark Canyon Formation, also referred to as the capping conglomerate, as a return to a braided river system (Fig. 11). Due to the similarity in sorting, grain size, rounding, and general lack of internal sedimentary structures between the bedded conglomerate facies observed in Stages 4 and 2, we interpret the capping conglomerate to represent deposition in a braided river system similar to that of Stage 2. Limited overall exposure (maximum ∼ 15 m preserved) and a lack of observable cyclicity in the capping conglomerates limits the identification of the exact type of braided river these deposits represent.

Basin Evolution

The deposition of the Newark Canyon Formation type section provides a unique perspective on the regional deformation history of the Central Nevada thrust belt and the broader Sevier hinterland region during the Cretaceous, as well as to other basins with similar styles of sedimentation. Sedimentation in piggyback basins is typically dominated by the competing factors of thrust-induced uplift, load-induced subsidence, and regional climate (Ori and Friend 1984; Coogan 1992; Talling et al. 1995; Currie 1998). Multiple lines of evidence suggest that the deposition and coeval deformation of the synorogenic Newark Canyon Formation was in response to the growth of folds and motion on associated east-vergent thrust faults proximal to the type section, principally the Eureka Culmination and the Strahlenberg anticline (Vandervoort 1987; Long et al. 2014; Long 2015; Di Fiori et al. 2020). The Newark Canyon Formation is interpreted to represent active sedimentation during progressive subsidence of the eastern limb of the east-vergent Strahlenberg anticline (Di Fiori et al. 2020). This is demonstrated by an intraformational shallow (∼ 17° W) over steep (∼ 40° W) bedding relationship within Stage 2 (Knc2–Knc3), as well as an angular unconformity where beds at the base of Stage 4 (Knc5) are ∼ 10–20° shallower than the underlying beds of Stages 1 to 3 (Knc1 to 4). This angular unconformity is observed within five separate outcrops of Stage 4 conglomerates that span a N–S distance of ∼ 4.5 km. U-Pb detrital-zircon geochronology suggests an ∼ 4 Myr gap between deposition of Stage 3 and Stage 4 (Di Fiori et al. 2020; Figs. 5B, 9). Thus, this angular unconformity demonstrates that the Newark Canyon Formation was deposited during long-term growth of two prominent east-vergent folds, the proximal Strahlenberg anticline and the more distal (∼ 10 to 15 km to the west), larger-scale Eureka Culmination, which are interpreted to be components of the Central Nevada thrust belt in the region of the type section (Di Fiori et al. 2020).

Changes in along-strike thicknesses in the Newark Canyon Formation are interpreted to be the result of changes in accommodation magnitude that were controlled by the development of proximal Central Nevada thrust belt structures, including the Strahlenberg anticline (Di Fiori et al. 2020, their Figs. 12 and 13). The Eureka Culmination, an anticline located 10 to 15 km to the west of the Newark Canyon Formation type section, was structurally elevated as much as ∼ 4–5 km relative to the surrounding region, and is interpreted to have been constructed synchronous with deposition of the Newark Canyon Formation (Long et al. 2014; Di Fiori et al. 2020). Clast compositions and provenance data from the Newark Canyon Formation (Di Fiori et al. 2020) preserve the sequential unroofing of Permian–Pennsylvanian, Mississippian, and Devonian stratigraphic units, which provides further evidence that sedimentation of the Newark Canyon Formation resulted from the progressive erosional denudation of the crest zone of the nearby Eureka Culmination. Paleocurrent directions determined from clast-imbrication analysis (Vandervoort 1987) further corroborate the interpretation that the fluvial systems of the type section accommodated east- to northeast-directed drainage of highlands to the west.

The changes in depositional environment through time preserved by the Newark Canyon Formation likely demonstrate that rates of regional contractional deformation were not uniform, which caused variation in the available accommodation and sediment supply. The gradient of the landscape and sediment supply into the Newark Canyon Formation piggyback basins to the east would likely have evolved mainly as a result of the progressive uplift of the Eureka Culmination and Strahlenberg anticline. At the base of the Newark Canyon Formation, the anastomosing system preserved in Stage 1 indicates a low-gradient environment that was at or near local base level (Makaske 2001). Anastomosing rivers with associated palustrine environments can be loosely classified as overfilled lacustrine systems according to the classification system of Carroll and Bohacs (1999). In this classification system, the type of lacustrine deposition is a function of the potential accommodation and the supply of sediment and water into the basin (Carroll and Bohacs 1999; Bohacs et al. 2000). Being an overfilled lacustrine system indicates that Stage 1 had a relatively small amount of potential accommodation in which sediment could be deposited. Together, the results of Di Fiori et al. (2020) and this study suggest that the presence of an anastomosing system and associated environments are evidence of initial growth of the Eureka Culmination.

The transition from an anastomosing system to the higher-energy braided river environment that characterizes Stage 2 indicates an increase in structural uplift along the Eureka Culmination resulting in higher stream competency and capacity associated with increased fluvial gradient in the Newark Canyon Basin. These changes in turn would have caused the fluvial system in the Newark Canyon piggyback basin to become choked with sediment, increased the average clast size, and reorganized the fluvial system into a braided river.

Interpreting the development of a lacustrine system in Stage 3 of the Newark Canyon Formation is difficult because there are several plausible mechanisms that could have resulted in the reorganization of a fluvial system into a balance-filled lacustrine environment. Talling et al. (1995) assessed the link between orogenic deformation and piggyback basin sedimentary patterns for the Late Cretaceous to Eocene Axhandle piggyback basin in Utah. Through sedimentary analysis and structural mapping, they inferred that formation of lacustrine and poorly drained alluvial deposits best correlated with periods of basin-margin uplift that would create new structural obstructions of drainage. This is a possible explanation for the development of a lacustrine system in the Newark Canyon Formation, although consistent east- to northeast-directed paleocurrents for conglomerates in Stage 2 and Stage 4 suggest that basin-wide drainage systems were not altered drastically. Alternatively, following the lacustrine interpretative model put forth by Carrol and

←

water indicate periods where the landscape is inundated with water and desiccating, respectively. **Stage 2**: Braided-river environment with several active fluvial channels that corresponds to Knc2–3. **Stage 3**: Lacustrine environment that corresponds to Knc4. Estimates of water height are difficult, but shoreline facies are not preserved in the type section, suggesting that the lake was tens of meters deep. Progressive dips of Knc1 through Knc3 are omitted for visual simplicity (Di Fiori et al. 2020). **Stage 4**: Braided-river system that corresponds to Knc5 Note that the map direction of the Stage 4 cross section differs from Stages 1–3 in order to show the angular unconformity between Knc1–4 and Knc5.

Bohacs (1999), a lacustrine system in Stage 3 could be the result of an increase in accommodation potentially due to subsidence in the piggyback basin while the sediment supply remained relatively constant. An increase in accommodation would allow for the development of a balance-filled lacustrine system and preservation of more fine-grained material relative to Stages 1 and 2 of the Newark Canyon Formation.

A fluvially reworked tuff at the top of the lacustrine deposits found in the TS3 section that has been dated at 103.0 ± 0.7 Ma using U-Pb zircon geochronology likely indicates the approximate timing of shutdown of the lacustrine system and the beginning of later erosion of the lake sediments (Di Fiori et al. 2020). The capping conglomerate of Stage 4 indicates that a final pulse of high-energy fluvial deposition occurred before sedimentation or preservation stopped. A detrital-zircon maximum depositional age estimated using U-Pb zircon geochronology from the capping conglomerate (98.6 ± 1.9 Ma; Di Fiori et al. 2020) demonstrates a major hiatus in deposition between Stage 3 and 4 in the type section. This unconformity suggests that the deposition of Stage 4 occurred at least ∼ 4 Myr after Stage 3.

The transition into the braided river system of Stage 4 requires the development of a similar depositional environment as Stage 2, indicating possible cyclicity within the overall system. During the Albian and early Turonian (∼ 105 to ∼ 90 Ma), the global climate state is thought to have been steadily warming towards the mid-Turonian Cretaceous Thermal Maximum (KTM) (Takashima et al. 2006; Huber et al. 2018). Although it is possible to have short-term cyclicity of climate superimposed upon long-term trends, little is known about the short-term scale of cyclicity for this time, particularly on land. The specific role of regional climatic forcing on sedimentation in the Newark Canyon Formation will be assessed in more detail using more quantitative paleoclimate proxy records in future studies. Fluctuations in the magnitude of regional deformation, however, have been well documented throughout the North American Cordillera (e.g., Wells et al. 2012), and specifically along the Central Nevada thrust belt (Taylor et al. 2000; Long et al. 2014; Long 2015; Di Fiori et al. 2020). Therefore, we interpret the capping conglomerate to represent the final pulse of sediment shed off of the Eureka Culmination into newly formed accommodation that resulted from possibly reinvigorated deformation in the system, rather than climatically-controlled cyclicity.

Comparison with Similar Terrestrial Basins

Comparison of the Newark Canyon Formation with other terrestrial sedimentary basins provides an important framework in which this basin can be better contextualized and provides helpful insights into how the influence of both tectonics and climate can be preserved in the geologic record. For example, the Late Cretaceous to early Eocene North Horn Formation preserved in the San Pitch Mountains, Utah, was deposited in a piggyback basin associated with active tectonic deformation along the Sevier fold–thrust belt (Lawton and Trexler 1991; Lawton et al. 1993). The North Horn Formation is composed of conglomerate, sheet sandstone, "redbeds," coal-bearing units, and calcareous siltstone units that were deposited by alluvial fans, varied fluvial, overbank, and open-lacustrine systems. Similar to the Newark Canyon Formation, the depositional patterns of the North Horn Formation were strongly controlled by episodic thrust activation, which was interpreted based on progressive unconformities preserved in the basal conglomerate, thinning and progressive rotation of the lower sandstone, stratigraphic composition, and crosscutting structural relations (Lawton and Trexler 1991; Lawton et al. 1993). Talling et al. (1995) found that rapid uplift during times of low rates of regional subsidence are commonly associated with channel-belt incision during the formation of well-drained, mature paleosols. Conversely, periods of basin uplift during times of greater regional subsidence are correlated to deposition of lacustrine, palustrine, and poorly drained floodplain environments (Talling et al. 1995). It should be noted, however, that while these are helpful general relationships, there is no one unique facies that corresponds to active regional uplift because of the competition between the relative rates of subsidence and uplift. Applying this interpretive framework to the Newark Canyon Formation supports the interpretations laid out above in the Depositional Models and Basin Evolution sections. The presence of palustrine, poorly drained floodplain, and lacustrine environments, such as those found in Stage 1 and Stage 3 of the Newark Canyon Formation, indicate times of greater regional subsidence along with basin uplift. The stacked conglomerates of Stage 2 and Stage 4 suggest an increase in sediment supply, due to rapid uplift during a period marked by low rates of regional subsidence.

Several other concurrent terrestrial sedimentary basins in the Western U.S. provide examples of how deposits and sedimentary architectures similar to the Newark Canyon Formation were formed in notably different tectonic regimes. An example of a coeval sedimentary unit is the Cretaceous Cedar Mountain Formation in Utah and Colorado. The Cedar Mountain Formation preserves terrestrial sedimentary units that are subdivided into the lower Buckhorn Conglomerate that were deposited by sandy to gravelly braided rivers, and an upper assemblage of interbedded alluvial sandstone and mudstone, and palustrine limestone, and pedogenic deposits (Currie 1998; Kirkland et al. 1999; Garrison et al. 2007; Ludvigson et al. 2015). The upper Cedar Mountain Formation preserves deposits with striking similarities to Stage 1 of the Newark Canyon Formation that include thin micritic limestone beds that indicate development of shallow lacustrine to palustrine environments, and weakly developed paleosols with some carbonate nodules that suggest deposition on a poorly drained fluvial and/or lacustrine plain. Furthermore, the laterally discontinuous nature of the channel bodies and general lack of accretion surfaces found in the upper Cedar Mountain Formation indicate that the main form of channel migration was by avulsion (Currie 1998). This is similar to our interpretation for Stage 1 of the Newark Canyon Formation where interbedded palustrine pebbly pelmicrite, mottled micrite, and calcareous conglomerate indicate an anastomosing river system with frequent avulsion events. While the sedimentary similarities between the Cedar Mountain and the Newark Canyon Formations are notable, they represent deposition in different tectonic settings. The upper section of the Cedar Mountain Formation was deposited as the foredeep became overfilled and onlapped onto the uplifted forebulge of the Sevier foreland basin (Currie 1998), while the Newark Canyon Formation preserves deposition within a syncontractional piggyback basin in the hinterland of the Sevier fold–thrust belt (Vandervoort 1987; Druschke et al. 2011; Long et al. 2014; Di Fiori et al. 2020; this study).

An additional example is found in the latest Jurassic to Early Cretaceous Apache Canyon Formation. Soreghan (1998) describes the Apache Canyon Formation as a mixed carbonate and siliciclastic lacustrine sequence that was deposited in the extensional Bisbee Basin in Arizona. The Apache Canyon Formation is interpreted as a lacustrine system that varies between shallow lacustrine with shoreline, gravity-flow, and deep-water suspension facies that were deposited in a half-graben. While deposited during a similar time as the Newark Canyon Formation, the Apache Canyon Formation represents deposition in a tectonic environment from fundamentally different from that of the syncontractional setting of the Newark Canyon Formation. Soreghan (1998) points to the very rapid, high-amplitude fluctuations in lake level seen through abrupt vertical juxtaposition of deep-water and shallow-water deposits at the decimeter scale to argue for a climatically controlled system. The cyclicity found in the Apache Canyon Formation is due to catchment-scale climatically driven changes in water level in the graben lake system that caused oscillations in the balance between evaporation and precipitation (Soreghan 1998). In contrast, we do not observe abrupt subfacies alterations in the lacustrine deposition in Stage 3 of the Newark Canyon Formation. The return to a similar braided river system in Stage 4 indicates a longer timescale of cyclicity in the Newark Canyon Formation. We

interpret the reestablishment of a braided river system in Stage 4 as indication of reinvigorated growth of the Eureka Culmination and the Strahlenberg anticline.

As seen through these examples, similar sedimentary units can develop under a variety of structural and tectonic conditions. These comparisons among terrestrial sedimentary basins can serve as useful reminders that lithologic packages alone cannot be used to assess the type of basin or driving factors of sedimentation. Analysis of lithologies, structural and stratigraphic relationships, broader structural setting, and climatic system must be holistically taken into account when attempting to disentangle the dominant drivers of terrestrial sedimentation.

CONCLUSIONS

Based on vertical and lateral facies associations, and optical and cathodoluminescence petrographic images, we present a revised depositional model for the Newark Canyon Formation that provides significant additions and clarification to the descriptions and interpretations of the carbonate facies. The Newark Canyon Formation preserves palustrine, fluvial, and lacustrine deposits that were deposited concurrently with deformation associated with development of the Eureka Culmination during the middle of the Cretaceous ($\sim$ 113 to 98 Ma). During Stage 1 of the type section, heterogeneous wetland environments deposited micrite between anastomosing river conglomerate channels suggesting that uplift of the Eureka Culmination was just beginning to develop ($\sim$ 113 Ma). A braided river system then dominated deposition in Stage 2, preserving bedded conglomerates and planar-bedded sandstones that indicates an increase in structural uplift along the nearby Eureka Culmination providing enhanced sediment supply and increased fluvial gradient in the proximal piggyback basin. Stage 3 is marked by fossiliferous mudstones and micrites from a large-scale, freshwater lacustrine system that indicates either a reorganization of drainage patterns due to new structural containment or an increase in accommodation potentially due to subsidence in the piggyback basin while the sediment supply remained relatively constant. After either a depositional hiatus or extensive erosion representing $\sim$ 10 Myr, Stage 4 demonstrates a likely reinitiation of deformation in the region and deposition of the final capping conglomerate. While we cannot yet determine the specific role of climate on the environmental changes preserved, we conclude, based on the overall tectonic setting and known variable episodes of deformation throughout the Sevier hinterland, that regional tectonics was the dominant control on the changes in depositional environment.

SUPPLEMENTAL MATERIALS

Supplemental materials are available from the SEPM Data Archive: https://www.sepm.org/supplemental-materials.

ACKNOWLEDGMENTS

We are thankful to A. Todd and K. Connolly for their assistance and hard work in the field. This work was improved through conversations in the field with P. Druschke, R. Hilton, J. Quade, and K. Rafferty. Funding for this work was provided by the U.S National Science Foundation (EAR-1524785) to K.E.S., S.P.L., and J.W.B. This material is based on work supported by the National Science Foundation Graduate Research Fellowship under Grant No. DGE-1650115 awarded to A.C.F. Any opinions, findings, and conclusions or recommendations expressed in this material are those of the author(s) and do not necessarily reflect the views of the National Science Foundation. This work benefitted from insightful comments and suggestions by two reviewers, V.P. Wright and B. Currie, the associate editor, G.A. Ludvigson, and corresponding editor, J.B. Southard.

REFERENCES

Abrahão, D., and Warme, J., 1990, Lacustrine and associated deposits in a rifted continental margin: Lower Cretaceous Lagoa Feia Formation, Campos Basin, Offshore Brazil, *in* Katz, B.J., ed., Lacustrine Basin Exploration: Case Studies and Modern Analogs: American Association of Petroleum Geologists, Memoir 50, p. 287–305.

Allen, J.R., 1970, Studies in fluviatile sedimentation: a comparison of fining-upwards cyclothems, with special reference to coarse-member composition and interpretation: Journal of Sedimentary Petrology, v. 40, p. 298–323.

Alonso-Zarza, A.M., 2003, Palaeoenvironmental significance of palustrine carbonates and calcretes in the geological record: Earth-Science Reviews, v. 60, p. 261–298.

Alonso-Zarza, A.M., and Dorado-Valiño, M., 2006, A recent analogue for palustrine carbonate environments: the Quaternary deposits of Las Tablas de Daimiel wetlands, Ciudad Real, Spain, *in* Alonso-Zarza, A.M., and Tanner, L.H., eds., Paleoenvironmental Record and Applications of Calcretes and Palustrine Carbonates: Geological Society of America, Special Paper 416, p. 153–168.

Alonso-Zarza, A.M., and Wright, V.P., 2010, Palustrine carbonates, carbonates in continental settings: facies, environments, and processes, *in* Alonso-Zarza, A.M., and Tanner, L.H., eds., Carbonates in Continental Settings: Facies, Environments, and Processes: Elsevier, p. 103–131.

Alonso-Zarza, A.M., Calvo, J.P., and García del Cura, M.A., 1992, Palustrine sedimentation and associated features, grainification and pseudo-microkarst, in the Middle Miocene (intermediate unit) of the Madrid Basin, Spain: Sedimentary Geology, v. 76, p. 43–61.

Arenas-Abad, C., Vaquez-Urbez, M., Pardo-Tirapu, G., and Sancho-Marcen, C., 2010, Fluvial and associated carbonate deposits, *in* Alonso-Zarza, A.M., and Tanner, L.H., eds., Carbonates in Continental Settings: Elsevier, p. 133–175.

Armenteros, I., and Daley, B., 1998, Pedogenic modification and structure evolution in palustrine facies as exemplified by the Bembridge limestone (late Eocene) of the Isle of Wight, southern England: Sedimentary Geology, v. 119, p. 275–295.

Barron, E.J., and Washington, W.M., 1982, Cretaceous climate: a comparison of atmospheric simulations with the geologic record: Palaeogeography, Palaeoclimatology, Palaeoecology, v. 40, p. 103–133.

Barron, E.J., Hay, W.W., and Thompson, S., 1989, The hydrologic cycle: a major variable during Earth history: Palaeogeography, Palaeoclimatology, Palaeoecology, v. 75, p. 157–174.

Bohacs, K.M., Carroll, A.R., Neal, J.E., and Mankiewicz, P.J., 2000, Lake-basin type, source potential, and hydrocarbon character: an integrated sequence-stratigraphic-geochemical framework, *in* Gierlowski-Kordesch, E.H., and Kelts, K.R., eds., Lake Basins through Space and Time: American Association of Petroleum Geologists, Studies in Geology 46, p. 3–34.

Bonde, J.W., Hilton, R.P., Jackson, F.D., and Druschke, P.A., 2015, Fauna of the Newark Canyon Formation (Lower Cretaceous), east-central Nevada: Geological Society of Nevada, Symposium, p. 139–150.

Bown, T.M., and Kraus, M.J., 1987, Integration of channel and floodplain suites, I. Developmental sequence and lateral relations of alluvial paleosols: Journal of Sedimentary Petrology, v. 57, p. 587–601.

Burbank, D.W., Beck, R.A., Raynolds, R.G.H., Hobbs, R., and Tahirkheli, R.A.K., 1988, Thrusting and gravel progradation in foreland basins: a test of post-thrusting gravel dispersal: Geology, v. 16, p. 1143–1146.

Burchfiel, B.C., Lipman, P.W., and Zoback, M.L., 1992, Introduction, *in* Burchfiel, B.C., Lipman, P.W., and Zoback, M.L., eds., The Cordilleran Orogen: Conterminous US: Geological Society of America, p. 1–6.

Burgener, L., Hyland, E., Huntington, K.W., Kelson, J.R., and Sewall, J.O., 2019, Revisiting the equable climate problem during the Late Cretaceous greenhouse using paleosol carbonate clumped isotope temperatures from the Campanian of the Western Interior Basin, USA: Palaeogeography, Palaeoclimatology, Palaeoecology, v. 516, p. 244–267.

Carroll, A.R., and Bohacs, K.M., 1999, Stratigraphic classification of ancient lakes: balancing tectonic and climatic controls: Geology, v. 27, p. 99–102.

Chase, C.G., Gregory-Wodzicki, K.M., Parrish, J.T., and DeCelles, P.G., 1998, Topographic history of the Wesern Cordillera of North America and controls on climate, *in* Crowley, T.J., and Burke, K.C., eds., Tectonic Boundary Conditions for Climate Reconstructions: New York, Oxford University Press, p. 73–99.

Coney, P.J., and Harms, T.A., 1984, Cordilleran metamorphic core complexes: Cenozoic extensional relics of Mesozoic compression: Geology, v. 12, p. 550–554.

Coogan, J.C., 1992, Structural evolution of piggyback basins in the Wyoming–Idaho–Utah thrust belt, *in* Link, P.K., Kentz, M.A., and Platt, L.B., eds., Regional Geology of Eastern Idaho and Western Wyoming: Geological Society of America, Memoir 179, p. 55–81.

Currie, B., 1998, Upper Jurassic–Lower Cretaceous Morrison and Cedar Mountain formations, NE Utah–NW Colorado; relationships between nonmarine deposition and early Cordilleran foreland-basin development: Journal of Sedimentary Research, v. 68, p. 632–652.

David, L., 1941, *Leptolepis nevadensis*, a new Cretaceous fish: Journal of Paleontology, v. 15, p. 318–321.

DeCelles, P.G., 2004, Late Jurassic to Eocene evolution of the Cordilleran thrust belt and foreland basin system, western U.S.A.: American Journal of Science, v. 304, p. 105–168.

DeCelles, P.G., 2009, Cyclicity in Cordilleran orogenic systems: Nature Geoscience, v. 2, p. 1–7.

DeCelles, P.G., and Coogan, J.C., 2006, Regional structure and kinematic history of the Sevier fold-and-thrust belt, central Utah: Geological Society of America, Bulletin, v. 118, p. 841–864

Dewey, J.F., and Bird, J.M., 1970, Mountain belts and new global tectonics: Journal of Geophysical Research, v. 75, p. 2625–2647.

Di Fiori, R.V., Long, S.P., Fetrow, A.C., Snell, K.E., Bonde, J., and Vervoort, J., 2020, Syn-contractional deposition of the Cretaceous Newark Canyon Formation, Diamond Mountains, Nevada: implications for strain partitioning within the Western U.S. Cordillera: Geosphere. v. 16, p. 1–21.

Dickinson, W.R., 2004, Evolution of the North American Cordillera: Annual Reviews of Earth and Planetary Sciences, v. 32, p. 13–45.

Dilek, Y., and Moores, E.M., 1999, A Tibetan model for the early Tertiary western United States: Geological Society of London, Journal, v. 156, p. 929–941.

Druschke, P., Hanson, A.D., Wells, M.L., Gehrels, G.E., and Stockli, D., 2011, Paleogeographic isolation of the Cretaceous to Eocene Sevier hinterland, east-central Nevada: insights from U-Pb and (U-Th)/He detrital zircon ages of hinterland strata: Geological Society of America, Bulletin, v. 123, p. 1141–1160.

Duchaufour, P., 1982, Hydromorphic soils, *in* Duchaufour, P., and Duchaufour, R., eds., Pedology: pedogenesis and classification: Springer, p. 335–372.

Dunagan, S.P., and Driese, S.G., 1999, Control of terrestrial stabilization on late Devonian palustrine carbonate deposition: Catskill Magnafacies, New York, U.S.A: Journal of Sedimentary Research, v. 69, p. 1–12.

Ernst, W.G., 2009, Rise and fall of the Nevadaplano: International Geology Review, v. 51, p. 583–588.

Fillmore, R.P., and Middleton, L.T., 1989, Tectonic and transport controls on conglomerate composition, Upper Cretaceous of southwest Utah, *in* Colburn, I.P., Abbott, P.L., and Minch, J., eds., Conglomerate in Basin Analysis: A Symposium Dedicated to A.O. Woodford: SEPM, Pacific Section, p. 113–122.

Flügel, E., 2004, Microfacies of Carbonate Rocks: Analysis, Interpretation and Application, 2nd Edition: Springer International Publishing, 996 p.

Folk, R.L., 1959, Practical petrographic classification of limestones: American Association of Petroleum Geologists, Bulletin, v. 43, p. 1–38.

Fouch, T.D., 1979, Character and paleogeographic distribution of Upper Cretaceous (?) and Paleogene nonmarine sedimentary rocks in east-central Nevada, *in* Armentrout, J.M., Cole, M.R., and TerBest, H., Jr., eds., Cenozoic Paleogeography of the Western United States: SEPM, Pacific Coast Section, Paleogeography Symposium 3, p. 97–112.

Fouch, T.D., Hanley, J.H., and Forester, R.M., 1979, Preliminary correlation of Cretaceous and Paleogene lacustrine and related nonmarine sedimentary and volcanic rocks in parts of the eastern Great Basin of Nevada and Utah, *in* Newman, G.W., and Goode, H.D., eds., Basin and Range Symposium and Great Basin Field Conference: Rocky Mountain Association of Petroleum Geologists and Utah Geological Association, p. 305–312.

Freytet, P., and Plaziat, J.C., 1982, Continental carbonate sedimentation and pedogenesis: Late Cretaceous and Early Tertiary of southern France: E. Schweizerbart'sche Verlagasbuchhandlung, Contributions to Sedimentology, v. 12, 213 p.

Freytet, P., and Verrecchia, E.P., 2002, Lacustrine and palustrine carbonate petrography: an overview: Journal of Paleolimnology, v. 27, p. 221–237.

García, A., and Chivas, A., 2006, Diversity and ecology of extant and Quaternary Australian charophytes (Charales): Cryptogamie Algologie, v. 27, p. 323–340.

Garrison, J.R., Brinkman, D., Nichols, D.J., Layer, P., Burge, D., and Thayn, D., 2007, A multidisciplinary study of the Lower Cretaceous Cedar Mountain Formation, Mussentuchit Wash, Utah: a determination of the paleoenvironment and paleoecology of the *Eolambia caroljonesa* dinosaur quarry: Cretaceous Research, v. 28, p. 461–494.

Gierlowski-Kordesch, E.H., 2009, Lacustrine carbonates, *in* Alonso-Zarza, A.M., and Tanner, L.H., eds., Carbonates in Continental Settings: Amsterdam, Elsevier, Developments in Sedimentology 61, p. 1–101.

Goddard, E.N., Trask, P.D., de Ford, R.K., Rove, O.N., Singewald, J.T., and Overbeck, R.M., 1984, Rock Color Chart: The Rock-Color Committee, Geological Society of America, Field Guide.

Grey, M., and Nickelsen, R., 1989, Pedogenic slickensides, indicators of strain and deformation processes in redbed sequences of the Appalachian foreland: Geology, v. 17, p. 72–75.

Held, I.M., and Soden, B.J., 2002, Water vapor feedback and global warming: Annual Review of Energy and the Environment, v. 25, p. 441–475.

Held, I.M., and Soden, B.J., 2006, Robust responses of the hydrological cycle to global warming: Journal of Climate, v. 19, p. 5686–5699.

Herlinger, R., Zambonato, E.E., and De Ros, L.F., 2017, Influence of diagenesis on the quality of Lower Cretaceous pre-salt lacustrine carbonate reservoirs from Northern Campos Basin, Offshore Brazil: Journal of Sedimentary Research, v. 87, p. 1285–1313.

Huber, B.T., MacLeod, K.G., Watkins, D.K., and Coffin, M.F., 2018, The rise and fall of the Cretaceous hot greenhouse climate: Global and Planetary Change, v. 167, p. 1–23.

Jaillard, B., Guyon, A., and Maurin, A.F., 1991, Structure and composition of calcified roots and their recognition in calcareous soils: Geoderma, v. 50, p. 197–210.

Jordan, T.E., and Allmendinger, R.W., 1986, The Sierra Pampeanas of Argentina: a modern analogue of Rocky Mountain foreland deformation: American Journal of Science, v. 286, p. 737–764.

Kirkland, J.I., Ciffeli, R.L., Britt, B.B., DeCourten, F.L., Eaton, J.G., and Parrish, J., 1999, Distribution of vertebrate faunas in the Cedar Mountain Formation, east-central Utah, *in* Gillette, D.D. ed., Vertebrate Paleontology in Utah: Utah Geological Survey, Miscellaneous Publication 99-1, p. 201–218

Klappa, C.F., 1980, Rhizoliths in terrestrial carbonates: classification, recognition, genesis and significance: Sedimentology, v. 27, p. 613–629.

Kraus, M.J., 1999, Paleosols in clastic sedimentary rocks: their geologic applications: Earth-Science Reviews, v. 47, p. 41–70.

Lasemi, Z., and Sandberg, P., 1993, Microfabric and compositional clues to dominant mud mineralogy of micrite precursors, *in* Rezak, R., and Lavoie, D., eds., Carbonate Microfabrics: New York, Springer-Verlag, p. 173–186.

Lawton, T.F., and Trexler, J.H., Jr., 1991, Piggyback basin in the Sevier orogenic belt, Utah: implications for development of the thrust wedge: Geology, v. 19, p. 827–830.

Lawton, T.F., Talling, P.J., Hobbs, R.S., Trexler, J.H., Jr., Weiss, M.P., and Burbank, D.W., 1993, Structure and stratigraphy of Upper Cretaceous and Paleogene strata (North Horn Formation), eastern San Pitch Mountains, Utah: sedimentation at the front of the Sevier orogenic belt: U.S. Geological Survey, Bulletin 1787-II, p. 1–33.

Leng, M.J., and Marshall, J.D., 2004, Palaeoclimate interpretation of stable isotope data from lake sediment archives: Quaternary Science Reviews, v. 23, p. 811–831.

Littler, K., Robinson, S.A., Bown, P.R., Nederbragt, A.J., and Pancost, R.D., 2011, High sea-surface temperatures during the Early Cretaceous Epoch: Nature Geoscience, v. 4, p. 169–172.

Long, S.P., 2015, An upper-crustal fold province in the hinterland of the Sevier orogenic belt, eastern Nevada, U.S.A.: a Cordilleran valley and ridge in the Basin and Range: Geosphere, v. 11, p. 404–424.

Long, S.P., 2019, Geometry and extension magnitude of the Basin and Range Province (39°N), Utah, Nevada, and California, USA: constraints from a province-scale cross section: Geological Society of America, Bulletin, v. 131, p. 1–21.

Long, S.P., Henry, C.D., Muntean, J.L., Edmondo, G.P., and Thomas, R.D., 2012, Preliminary Geologic Map of the Southern Eureka Mining District, Eureka and White Pine Counties, Nevada: Nevada Bureau of Mines and Geology, Nevada Geological Survey, Plate 2 of 2, scale 1:24,000.

Long, S.P., Henry, C.D., Muntean, J.L., Edmondo, G.P., and Cassel, E.J., 2014, Early Cretaceous construction of a structural culmination, Eureka, Nevada, U.S.A.: implications for out-of-sequence deformation in the Sevier hinterland: Geosphere, v. 10, p. 564–584.

Long, S.P., Thomson, S.N., Reiners, P.W., and Di Fiori, R.V., 2015, Synorogenic extension localized by upper-crustal thickening: an example from the Late Cretaceous Nevadaplano: Geology, v. 43, p. 351–354.

Lorenz, J.C., and Gavin, W., 1984, Geology of the Two Medicine Formation and sedimentology of a dinosaur nesting ground: Montana Geological Society, Field Conference and Symposium, Guidebook, p. 175–186.

Ludvigson, G.A., Joeckel, R.M., Murphy, L.R., Stockli, D.F., González, L.A., Suarez, C.A., Kirkland, J.I., and Al-Suwaidi, A.H., 2015, The emerging terrestrial record of Aptian–Albian global change: Cretaceous Research, v. 56, p. 1–24.

Mack, G.H., James, W.C., and Monger, H.C., 1993, Classification of paleosols: Geological Society of America, Bulletin, v. 105, p. 129–136.

MacNeil, F.S., 1939, Fresh-water invertebrates and land plants of Cretaceous age from Eureka Nevada: Journal of Paleontology, v. 13, p. 355–360.

Makaske, B., 2001, Anastomosing rivers: a review of their classification, origin and sedimentary products: Earth-Science Reviews, v. 53, p. 149–196.

Martin, C.A.L., and Turner, B.R., 1999, Origins of massive-type sandstones in braided river systems: Earth-Science Reviews, v. 44, p. 15–38.

Marty, D., and Meyer, C.A., 2006, Depositional conditions of carbonate-dominated palustrine sedimentation around the K-T boundary (Faciès Rognacien, northeastern Pyrenean foreland, southwestern France), *in* Alonso-Zarza, A.M., and Tanner, L.H., eds., Paleoenvironmental Record and Applications of Calcretes and Palustrine Carbonates: Geological Society of America, Special Paper 416, p. 169–187.

Miall, A.D., 1977a, A review of the braided river depositional environment: Earth-Science Reviews, v. 13, p. 1–62.

Miall, A.D., 1977b, Lithofacies types and vertical profile models in braided river deposits: a summary: Fluvial Sedimentology, p. 597–604.

Mintz, J.S., Driese, S.G., Breecker, D.O., and Ludvigson, G.A., 2011, Influence of changing hydrology on pedogenic calcite precipitation in vertisols, Dance Bayou, Brazoria County, Texas, U.S.A.: implications for estimating paleoatmospheric pCO_2: Journal of Sedimentary Research, v. 81, p. 394–400.

Murru, M., Ferrara, C., and Matteucci, R., 2015, Paleocene palustrine and ephemeral alluvial facies in southern Sardinia (Italy): Italian Journal of Geosciences, v. 134, p. 134–148.

Nadon, G.C., 1994, The genesis and recognition of anastomosed fluvial deposits: data from the St. Mary River Formation, southwestern Alberta, Canada: Journal of Sedimentary Research, v. 64, p. 451–463.

Nanson, G.C., and Croke, J.C., 1992, A genetic classification of floodplains: Geomorphology, v. 4, p. 459–486.

Nolan, T.B., and Hunt, R.N., 1962, The Eureka Mining District, Nevada: U.S. Geological Survey, Professional Paper 406, p. 1–75.

Nolan, T.B., Merriam, C.W., and Williams, J.S., 1956, The stratigraphic section in the vicinity of Eureka, Nevada: U.S. Geological Survey, Professional Paper 276, p. 1–73.

Nolan, T.B., Merriam, C.W., and Blake, M.C.J., 1974, Geologic Map of Pinto Summit Quadrangle, Eureka and White Pine Counties, Nevada: U.S. Geological Survey, Miscellaneous Investigations Series, Map I-793, scale 1:31,680.

NRCS Soils Staff, 2017, Examination and description of soil profiles: Soil Survey Manual, U.S. Department of Agriculture, p. 1–79.

Ori, G., and Friend, P.F., 1984, Sedimentary basins formed and carried piggyback on active thrust sheets: Geology, v. 12, p. 475–478.

Pagani, M., Huber, M., and Sageman, B., 2013, Greenhouse climates, *in* Holland, H.D., and Turekian, K.K., eds., Treatise on Geochemistry: Elsevier, p. 281–304.

Pagel, M., Barbin, V., Blanc, P., and Ohnenstetter, D., 2000, Cathodoluminescence in Geosciences: an introduction: Springer-Verlag, 21 p.

Parrish, J.T., Hasiotis, S.T., and Chan, M.A., 2017, Carbonate deposits in the Lower Jurassic Navajo Sandstone, southern Utah and northern Arizona: Journal of Sedimentary Research, v. 87, p. 740–762.

Pederson, J., Pazzaglia, F., Smith, G., and Mou, Y., 2000, Neogene through Quaternary hillslope records, basin sedimentation, and landscape evolution of southeastern Nevada, in Great Basin and Sierra Nevada, *in* Lageson, D., Peters, S., and Lahren, M., eds., Geological Society of America, Field Guide 2, p. 117–143.

Platt, N.H., 1989, Lacustrine carbonates and pedogenesis: sedimentology and origin of palustrine deposits from the Early Cretaceous Rupelo Formation, W Cameros Basin, N Spain: Sedimentology, v. 36, p. 665–684.

Quigley, M.C., Sandiford, M., and Cupper, M.L., 2007, Distinguishing tectonic from climatic controls on range-front sedimentation: Basin Research, v. 19, p. 491–505.

Richardson, J.L., and Vepraskas, M.J., 2001, Wetland Soils: Genesis, Hydrology, Landscapes, and Classification: Boca Ratón, CRC Press, 417 p.

Roberts, R.J., Montgomery, K.M., and Lehner, R.E., 1967, Geology and mineral resources of Eureka County, Nevada: Nevada Bureau of Mines and Geology, Bulletin, v. 64, 164 p., 11 plates.

Royer, D.L., 2006, CO_2-forced climate thresholds during the Phanerozoic: Geochimica et Cosmochimica Acta, v. 70, p. 5665–5675.

Rust, B.R., 1972, Structure and process in a braided river: Sedimentology, v. 18, p. 221–245.

Sacristán-Horcajada, S., Arribas, M.E., and Mas, R., 2016, Pedogenetic calcretes in early syn-rift alluvial systems (Upper Jurassic, West Cameros Basin), northern Spain: Journal of Sedimentology Research, v. 86, p. 268–286.

Sanjuan, J., and Martín-Closas, C., 2012, Charophyte palaeoecology in the Upper Eocene of the Eastern Ebro basin (Catalonia, Spain): biostratigraphic implications: Palaeogeography, Palaeoclimatology, Palaeoecology, v. 365–366, p. 247–262.

Smith, D.G., 1983, Anastomosed fluvial deposits: modern examples from western Canada, *in* Collinson, J.D., and Lewin, J., eds., Modern and Ancient Fluvial Systems: International Association of Sedimentologists, p. 155–168.

Smith, D.G., 1986, Anastomosing river deposits, sedimentation rates and basin subsidence, Magdalena River, Northwestern Colombia, South America: Sedimentary Geology, v. 46, p. 177–196.

Smith, D.G., 1987, Meandering river point bar lithofacies models: modern and ancient examples compared, *in* Ethridge, F.K., Flores, R.M., and Harvey, M.D., eds., Recent Developments in Fluvial Sedimentology: SEPM, Special Publication 39, p. 83–91.

Smith, D.G., and Smith, N.D., 1980, Sedimentation in anastomosed river systems: examples from alluvial valleys near Banff, Alberta: Journal of Sedimentary Petrology, v. 50, p. 157–164.

Smith, J.K., and Kettner, K.B., 1976, Stratigraphy of post-Paleozoic rocks and summary of resources in the Carlin–Pinon Range area, Nevada, with a section on aeromagnetic survey: U.S. Geological Survey, Professional Paper 867-B, 47 p.

Snell, K.E., Koch, P.L., Druschke, P., Foreman, B.Z., and Eiler, J.M., 2014, High elevation of the "Nevadaplano" during the Late Cretaceous: Earth and Planetary Science Letters, v. 386, p. 52–63.

Soreghan, M., 1998, Facies distributions within an ancient asymmetric lake basin: the Apache Canyon Formation, Bisbee Basin, Arizona, *in* Pitman, J.K., and Carroll, A.R., eds., Modern and Ancient Lake Systems: New Problems and Perspectives: Utah Geological Association, Guidebook 26, p. 163–190.

Soulié-Märsche, I., and García, A., 2015, Gyrogonites and oospores, complementary viewpoints to improve the study of the charophytes (Charales): Aquatic Botany, v. 120, p. 7–17.

Strawson, F.M., 1981, The geology of the Permian Carbon Ridge Formation, east-central Nevada [MS Thesis]: University of Nevada–Reno, 139 p.

Suarez, M.B., González, L.A., and Ludvigson, G.A., 2011, Quantification of a greenhouse hydrologic cycle from equatorial to polar latitudes: the mid-Cretaceous water bearer revisited: Palaeogeography, Palaeoclimatology, Palaeoecology, v. 307, p. 301–312.

Takashima, R., Nishi, H., Huber, B.T., and Leckie, R.M., 2006, Greenhouse World and the Mesozoic Ocean: Oceanography, v. 19, p. 64–74.

Talling, P.J., Lawton, T.F., Burbank, D.W., and Hobbs, R.S., 1995, Evolution of latest Cretaceous–Eocene nonmarine deposystems in the Axhandle piggyback basin of central Utah: Geological Society of America, Bulletin, v. 107, p. 297–315.

Taylor, W.J., Bartley, J.M., Martin, M.W., Geissman, J.W., Walker, J.D., Armstrong, P.A., and Fryxell, J.E., 2000, Relations between hinterland and foreland shortening: Sevier orogeny central North American Cordillera: Tectonics, v. 19, p. 1124–1143.

Tucker, M.E., and Wright, V.P., 1990, Carbonate Sedimentology: Blackwell Publishing, 482 p.

Ufnar, D.F., González, L.A., Ludvigson, G.A., Brenner, R.L., and Witzke, B.J., 2004, Evidence for increased latent heat transport during the Cretaceous (Albian) greenhouse warming: Geology, v. 32, p. 1049–1052.

Van Buer, N.J., Miller, E.L., and Dumitru, T.A., 2009, Early Tertiary paleogeologic map of the northern Sierra Nevada batholith and the northwestern Basin and Range: Geology, v. 37, p. 371–374.

Vandervoort, D.S., 1987, Sedimentology, provenance, and tectonic implications of the Cretaceous Newark Canyon Formation [MS Thesis]: Montana State University, Bozeman, 135 p.

Vandervoort, D.S., and Schmitt, J.G., 1990, Cretaceous to early Tertiary paleogeography in the hinterland of the Sevier thrust belt, east-central Nevada: Geology, v. 18, p. 567–570.

Wang, Y., Huang, C., Sun, B., Quan, C., Wu, J., and Lin, Z., 2014, Paleo-CO_2 variation trends and the Cretaceous greenhouse climate: Earth-Science Reviews, v. 129, p. 136–147.

Wells, M.L., Hoisch, T.D., Cruz-Uribe, A.M., and Vervoort, J.D., 2012, Geodynamics of synconvergent extension and tectonic mode switching: constraints from the Sevier–Laramide orogen: Tectonics, v. 31, p. 1–20.

Williams, P.F., and Rust, B.R., 1969, The Sedimentology of a braided river: Journal of Sedimentary Petrology, v. 39, p. 649–679.

Wright, V.P., 1989, Terrestrial stromatolites and laminar calcretes: a review: Sedimentary Geology, v. 65, p. 1–13.

Wright, V.P., 1992, A revised classification of limestones: Sedimentary Geology, v. 76, p. 177–185.

Wright, V.P., and Peeters, C., 1989, Origins of some Early Carboniferous calcrete fabrics revealed by cathodoluminescence: implications for interpreting the sites of calcrete formation: Sedimentary Geology, v. 65, p. 345–353.

Wright, V.P., and Platt, N.H., 1995, Seasonal wetland carbonate sequences and dynamic catenas: a re-appraisal of palustrine limestones: Sedimentary Geology, v. 99, p. 65–71.

Wright, V.P., Platt, N.H., Marriott, S.B., and Beck, V.H., 1995, A classification of rhizogenic (root-formed) calcretes, with examples from the Upper Jurassic–Lower Cretaceous of Spain and Upper Cretaceous of southern France: Sedimentary Geology, v. 100, p. 143–158.

Wright, V.P., Zarza, A.M.A., Sanz, M.E., and Calvo, J.P., 1997, Diagenesis of late Miocene micritic lacustrine carbonates, Madrid Basin, Spain: Sedimentary Geology, v. 114, p. 81–95.

Wright, V.P., Taylor, K.G., and Beck, V.H., 2000, The paleohydrology of Lower Cretaceous seasonal wetlands, Isle of Wight, southern England: Journal of Sedimentary Research, v. 70, p. 619–632.

Yonkee, W.A., and Weil, A.B., 2015, Tectonic evolution of the Sevier and Laramide belts within the North American Cordillera orogenic system: Earth-Science Reviews, v. 50, p. 531–593.

Received 7 August 2019; accepted 7 April 2020.